

Optimal control of connected autonomous vehicles in a mixed traffic corridor

Wenbo Sun, Fangni Zhang, Wei Liu, and Qingying He

Abstract—This paper investigates the potential of improving the overall traffic and energy efficiency by properly controlling a proportion of controllable connected and autonomous vehicles (CAVs) in a mixed traffic corridor. Specifically, we develop a control framework that optimizes controllable CAV trajectories taking into account other vehicles for simultaneously improving traffic throughput and reducing the total energy consumption of all vehicles. The property of the control framework is firstly analytically examined in a simplified and tractable scenario where a human-driven vehicle (HV) follows a CAV. We found that the optimal acceleration is larger if one emphasizes more on improving travel distance within the optimization horizon, or smaller when one emphasizes more on saving energy. The continuous-time optimization model formulation is then discretized, which is solved for real-time application in a model predictive control (MPC) fashion. In numerical studies, the proposed method is tested in various scenarios, e.g., with/without an intersection, under different proportions of controllable CAVs, possible vehicle permutations, and varying overall traffic intensities. Numerical results show that the normalized energy consumption can be reduced by up to 45% and the average travel time reduced by 65%, showing a significant improvement in the road throughput. Notably, even with a limited number of controllable CAVs, the proposed method can achieve a promising performance, e.g., about 20% controllable CAVs can achieve half the benefits of a fully controllable CAV environment.

Index Terms—Connected and autonomous vehicle (CAV), Mixed traffic, Traffic throughput, Energy consumption, Trajectory optimization.

I. INTRODUCTION

CONNECTED and autonomous vehicles (CAVs) have drawn a lot of attention in recent decades [1]. Many studies have shown that CAVs have a great potential of improving traffic efficiency [1], reducing energy consumption [2], and alleviating parking congestion [3]. It is also expected that there will be a transition period where CAVs share the road with traditional human-driven vehicles (HVs) in the near future. Even if all vehicles are replaced by CAVs, some vehicles might not be fully controllable by one centralized controller due to privacy concerns or other issues. Recently, many studies suggested that CAVs with distributed control can

This study was supported by The University of Hong Kong (No. 202009185002), the National Natural Science Foundation of China (No. 72101222), and the Research Grants Council of Hong Kong (No. 27202221) and the National Natural Science Foundation of China / Research Grants Council of Hong Kong Joint Research Scheme (N_PolyU521/22). (Corresponding author: Fangni Zhang.)

Wenbo Sun and Fangni Zhang are with the Department of Industrial and Manufacturing Systems Engineering, University of Hong Kong, Hong Kong, China (e-mail: sunwb@connect.hku.hk; fnzhang@hku.hk).

Wei Liu and Qingying He are with the Department of Aeronautical and Aviation Engineering, The Hong Kong Polytechnic University, Hong Kong, China (e-mail: wei.w.liu@polyu.edu.hk; qingying.he@polyu.connect.hk).

achieve significant benefits in energy consumption by driving proactively in response to traffic states in a traffic corridor [4], [5]. However, little attention was paid to the potential benefits of controlling a limited number of CAVs in a mixed traffic flow.

In this context, this study investigates the potential of improving the overall traffic and energy efficiency by only controlling a proportion of vehicles, i.e., controllable CAVs. Particularly, this paper develops a control framework to optimize controllable CAVs' trajectories in a mixed traffic corridor. Other vehicles, including uncontrollable CAVs and human-driven vehicles (HVs), are not controllable by the controller. According to the level of automation and the class of cooperation defined by [6], CAVs in this paper refer to those with at least automation level 3, i.e., having automated driving capacity in specific conditions. Meanwhile, CAVs are in cooperation class C or above so that they can drive proactively in coordination with other road users, which include other CAVs and HVs.

Many studies examined the CAV trajectory control in a fully CAV environment [7], [8]. However, a transition period with mixed CAVs and HVs is expected before a fully CAV environment can be achieved and there is an imperative need to come up with effective control strategies to cope with the mixed traffic during the transition. In the mixed traffic context, the model predictive control (MPC) framework can be adopted to optimize CAV trajectories according to predicted traffic states.¹ In particular, the interactions between CAVs and HVs and the responses of HVs to CAVs are important considerations. Along this line, some studies adopted car-following models such as the intelligent driver model (IDM) [11] and the optimal velocity model [12] to model the interactions between individual vehicles [13]. The HV trajectories were predicted by a shooting heuristic method in the optimization of CAVs' trajectories in [14].

Most studies on CAV trajectory optimization in the mixed traffic context aim at minimizing the cost of target CAV(s). Very few considered the cost of other vehicles in the mixed traffic flow. The understanding of the system-wide effects of CAVs on the whole traffic flow remains limited. Although some studies have shown that optimized CAVs can smooth traffic and potentially benefit the following vehicles [15], [16], how to improve overall traffic efficiency and reduce energy

¹In addition to trajectory control, the impacts of CAVs on network traffic equilibrium have been investigated from different aspects, e.g., the design of dedicated CAV lanes [9], CAV parking behavior [3], and the CAV routing problem [10].

consumption by controlling a limited number of CAVs is not fully clear.

Existing studies of CAV trajectory control for traffic efficiency often assumed the formation of vehicle platoons. Consequently, the traffic efficiency can be improved by appropriately managing these platoons [2], [17]. Different types of platoons have been examined. For example, Zhao et al. [12] separated the mixed traffic flow into multiple platoons led by CAVs, and the centralized controller controls the lead CAV with the objective of minimizing the fuel consumption of the platoon to pass a signalized intersection. Gong & Du [18] dealt with a mixed-vehicle platoon, consisting of an HV platoon sandwiched by two CAV platoons. Based on a mixed vehicle platoon, Guo et al. [14] jointly optimized the CAV trajectories and the Signal Phase and Timing (SPaT) at intersections where HV trajectories are constructed by a shooting heuristic method. Leveraging the traffic flow model, Piacentini et al. [19] proposed to reduce the energy consumption of the mixed traffic flow by controlling a CAV platoon as a moving bottleneck. In [20], the mixed traffic flow is divided into several sub-vehicle platoons consisting of a lead HV followed by several CAVs. Each sub-vehicle platoon is optimized by a deep reinforcement learning method. However, the ‘platoon-based’ methods require a certain CAV penetration rate for platoon formation, which may fail at low CAV penetration rates, especially in a mixed traffic corridor or with limited CAVs. Moreover, existing methods entail large computation burdens, making them difficult to be implemented in real-time.

The main contributions of this paper can be summarized as follows.

First, instead of controlling a single CAV, this study develops a control framework to improve traffic and energy efficiency by controlling a proportion of CAVs in a traffic corridor. The proposed method is implemented in an MPC fashion that can handle uncertainties, where the optimized trajectory keeps updating based on the current traffic information. In particular, the proposed method does not rely on forming a platoon and can be applied in various traffic scenarios with different numbers of controllable CAVs.

Second, this is the first study in the literature that investigates the analytical properties of the control method in a two-vehicle scenario, where an HV follows a CAV. We derive and analyze the optimal acceleration of the lead CAV under different conditions. Generally, the optimal acceleration increases with weighting factors for travel distance, but decreases with weighting factors for energy consumption.

Third, we develop solution approaches for the proposed method and systematically evaluate it under various traffic scenarios. Numerical results show that the average travel time and average energy cost of all vehicles can be significantly reduced in different traffic conditions, even with a low proportion of controllable CAVs. The promising results show the robustness and effectiveness of the proposed method, and shed light on the CAV cooperative control in mixed traffic corridors.

The remainder of this paper is organized as follows. Section II presents the proposed control framework as well as the analytical solution to a simple scenario. Section III examined the proposed method in different traffic scenarios/settings.

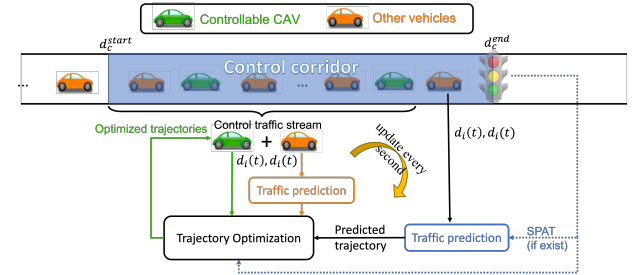


Fig. 1. Illustration of the control framework.

Section IV concludes the paper and discusses future work.

II. PROBLEM FORMULATION

This paper proposes a control method to improve traffic and energy efficiency with a limited number of CAVs in a mixed traffic corridor. As shown in Fig. 1, we consider a control traffic corridor with a single lane starting from \$d_c^{start}\$ to \$d_c^{end}\$, in which a proportion of CAVs are controllable, i.e., the controllable CAVs (in green). Other vehicles (in orange), including uncontrollable CAVs and HVs, are randomly distributed and drive in the control corridor without lane changing. The control corridor is equipped with relevant devices (e.g., the Dedicated Short Range Communication systems and roadside detectors such as cameras, lidars, and radars) that collect traffic information and inform the centralized controller of the vehicle and SPaT status within the control corridor in real-time. The control framework takes the traffic information as the control input, and the output is the trajectories of all controllable CAVs. Specifically, the centralized controller optimizes the trajectories of controllable CAVs to reduce the energy consumption of all vehicles and improve road throughput. The trajectories of other vehicles are predicted by the car-following models and serve as safety constraints in the optimization problem. Considering a control traffic stream led by the first controllable CAV, different prediction models may be adopted for uncontrollable vehicles inside or outside the control traffic stream to strike a balance between prediction accuracy and computation efficiency. To deal with potential uncertainties in the traffic flow, the proposed control method is implemented in the MPC fashion, where we solve and update the optimal decisions every \$T_{UD}\$ seconds (set as 1s in this paper). At each update instance, the optimization problem is solved for the next \$T_{OH}\$ seconds, referred to as the optimization horizon and \$T_{OH} \geq T_{UD}\$.

A. Model formulation

As shown in Fig. 1, we consider a control traffic stream starting with a controllable CAV. \$N(t)\$, \$N_c(t)\$, and \$N_h(t)\$ denote the sets of all vehicles, controllable CAVs, and other vehicles, respectively, and \$N(t) = N_c(t) \cup N_h(t)\$. The vehicles in \$N(t)\$ are numbered from the downstream to the upstream such that \$N(t) = \{1, 2, 3, \dots, n(t) - 1, n(t)\}\$, where \$n(t)\$ denotes the number of vehicles in the control traffic stream at time \$t\$. The main notations are listed in Appendix A.

For any vehicle $i \in N(t)$, $d_i(t)$ and $v_i(t)$ represent its location and speed at time t , respectively. The state of all vehicles in a mixed traffic flow at time t is defined as:

$$\mathbf{x}(t) = [d_1(t), v_1(t), \dots, d_{n(t)}(t), v_{n(t)}(t)]^T. \quad (1)$$

The system dynamic equation is given by:

$$\dot{\mathbf{x}}(t) = \frac{d\mathbf{x}(t)}{dt} = [v_1(t), a_1(t), \dots, v_{n(t)}(t), a_{n(t)}(t)]^T, \quad (2)$$

where $\dot{\mathbf{x}}(t)$ is the changing rate of the state $\mathbf{x}(t)$ with respect to time t ; $a_i(t)$ is the acceleration of vehicle i at time t .

To minimize the total cost of all vehicles in the control corridor, the objective function is defined as follows:

$$\min_{a_i, i \in N_c(t_0)} J = (-w_1)\Phi + w_2 \int_{t_0}^{t_f} \mathcal{L} dt, \quad (3a)$$

$$\text{where } \Phi(\mathbf{x}(t_f)) = \sum_{i=1}^{n(t_0)} d_i(t_f); \quad (3b)$$

$$\mathcal{L}(\mathbf{x}(t), \mathbf{u}(t), t) = \sum_{i=1}^{n(t_0)} a_i^2(t). \quad (3c)$$

The objective function (3a) consists of two terms: the total travel distance of all vehicles, Φ , and the total energy consumption of all vehicles, $\int_{t_0}^{t_f} \mathcal{L} dt$, during the optimization horizon. t_0 and t_f represent the start time and end time of the optimization horizon, respectively; $\mathbf{u}(t)$ is the control input, which is the acceleration of all controllable CAVs in (2).

The two terms are connected by weighting factors, $(-w_1)$ and w_2 . Given that a longer total travel distance in the optimization horizon means a larger traffic throughput, a negative weighting factor is applied to the first term (total travel distance) in the minimization problem (3a). The second term defined in (3c) is the acceleration square of all vehicles, representing the total energy consumption as well as the comfort cost. Previous studies have shown that square-of-acceleration can provide a good approximation of energy consumption in optimizing trajectories [21], [22], and sharp acceleration and deceleration may cause discomfort for passengers [23]. Moreover, this term allows for analytical tractability in the simplified scenario, which is investigated in Section II-B. The weighting factors are selected to normalize the two cost terms in the objective function, whereas the numerical results using different weighting factors are presented in Appendix IV. Specifically, we set $w_1 = 1 / \sum_{i=1}^{n(t_0)} (v_i(t_0) \cdot (t_f - t_0))$, where the denominator is the travel distance of all vehicles traveling at the initial speed during the optimization horizon; $w_2 = 1 / (n(t_0) \cdot (t_f - t_0))$, which means that each vehicle's speed may fluctuate with an acceleration rate of $1m/s^2$. Other combinations of weighting factors can also be adopted depending on the purpose of the centralized controller.

The optimization problem is subject to the following constraints.

1) Car-following model for uncontrollable vehicles:

Each vehicle should follow the system dynamics governed by (2), which indicates that the accelerations determine the trajectories of vehicles. In this paper, we consider that the accelerations of controllable CAVs in the control corridor are optimized by the centralized controller. The accelerations of other

vehicles are modeled by the Gazis-Herman-Rothery (GHR) car-following model in the optimization problem (3) [24]:

$$a_i(t) = (v_{i-1}(t) - v_i(t)) / \tau + s_i(t), \quad \forall i \in N_h(t), \quad (4)$$

where τ is the adaptation time which means the following vehicle tends to reach the same speed as its preceding vehicle in τ seconds. $s_i(t)$ is a slack variable, which would be 0 unless the GHR model cannot satisfy safety constraints (5). The GHR model allows for analytical tractability where the analytical properties of the model can be examined. Other more accurate car-following models can be readily incorporated into the proposed framework (e.g., IDM), however, the more complex model will result in a large computation burden.

2) Safety constraints:

To ensure safe car-following distance, we have the following constraints:

$$d_{i-1}(t) - d_i(t) \geq h \cdot v_i(t) + h_{min} - l_i(t), \quad \forall i \in N(t), \quad (5)$$

where h is the time headway; h_{min} is the minimum following distance when the vehicle is stationary; and $l_i(t)$ is a positive slack variable to allow slight violations near the constraint boundary.

The safe time headway h may be different in different car-following scenarios. In general, time headway consists of perception time and reaction time [25]. It normally takes human drivers 1s to 1.5s to take actions after perceiving the changes of traffic conditions. Thanks to the sensitive sensors onboard, CAVs can have smaller perception time [2]. Furthermore, when a CAV follows a CAV, both perception time and reaction time can be almost zero because the preceding CAV can broadcast its intended trajectory to the CAV behind [26], which means two CAVs can travel safely with a small following distance. Thus, different h values are assigned to the scenarios accordingly.

3) Signal constraints:

The proposed model intends to control CAVs in a general traffic corridor regardless of the existence of a signalized intersection. When there is an intersection inside the corridor, the signal constraints need to be incorporated into the optimization problem.

$$d_i(t) > d_{sig} \quad \text{or} \quad d_i(t) < d_{sig}, \quad \forall i \in N(t) \text{ and all } t \{t : sig(t) = red\}, \quad (6)$$

where d_{sig} is the location of the intersection; and $sig(t)$ represents the phase of the signal at time t , which can take the value of either red or green. Overall, (6) says that when the signal is red, all vehicles either passed the signal already or stopped before the signal. Thus, (6) governs that vehicles can only pass the intersection when the signal is not red. Notably, in this paper, the yellow phase (if exists) is lumped with red phases, and vehicles cannot pass the intersection with a yellow signal to ensure safety.

4) Speed and acceleration bounds:

Neither the vehicle speed $v_i(t)$ nor acceleration $a_i(t)$ can exceed the lower and upper bounds:

$$v_{min} \leq v_i(t) \leq v_{max}, \quad \forall i \in N(t), \quad (7a)$$

$$a_{min} \leq a_i(t) \leq a_{max}, \quad \forall i \in N(t), \quad (7b)$$

where v_{min} , v_{max} , a_{min} , a_{max} denote the lower and upper bounds of the vehicle speed and acceleration, respectively.

B. Analytical solutions and analysis

This section examines the analytical properties of the CAV trajectory optimization problem defined above. The general optimization problem is analytically intractable as it is highly nonlinear with numerous decision variables and differentiation/integration terms. In order to obtain the closed-form solution and derive analytical insights, we consider a simplified two-vehicle scenario, where an HV follows a CAV.

In the two-vehicle scenario, the objective function (3a) becomes:

$$\begin{aligned} \min_{a_1(t)} J_{\text{veh}} = & -w_{11}d_1(t_f) - w_{12}d_2(t_f) \\ & + \int_{t_0}^{t_f} (w_{21}a_1(t)^2 + w_{22}a_2(t)^2) dt, \end{aligned} \quad (8)$$

where $d_1(t_f)$ and $d_2(t_f)$ represent the travel distance during the optimization horizon of the lead CAV and the following HV, respectively; the control input is the acceleration of the lead CAV, i.e., $a_1(t)$. To better illustrate the effects of different cost components, we employ different weighting factors for the two vehicles. w_{11} and w_{12} are the weighting factors for the travel distance of the lead CAV and the following HV, respectively. w_{21} and w_{22} are associated with the energy consumption of the lead CAV and the following HV, respectively. Without loss of generality, we set the start time of the optimization horizon $t_0 = 0$.

We solve this optimization problem using PMP [27]. The Hamiltonian function \mathcal{H} is defined as:

$$\begin{aligned} \mathcal{H}(\mathbf{x}, a_1, \boldsymbol{\lambda}, t) = & \lambda_1(t)v_1(t) + \lambda_2(t)a_1(t) + \lambda_3(t)v_2(t) \\ & + \lambda_4(t)a_2(t) + w_{21}a_1(t)^2 + w_{22}a_2(t)^2, \end{aligned} \quad (9)$$

where $\boldsymbol{\lambda} = [\lambda_1, \lambda_2, \lambda_3, \lambda_4]^T$ is the co-state vector. It represents the shadow price of the associated state $\mathbf{x} = [d_1, v_1, d_2, v_2]$, which reflects the additional cost incurred by an incremental increase in the associated state \mathbf{x} .

According to the PMP, the optimal control $a_1^*(t)$ must satisfy:

$$\mathcal{H}(\mathbf{x}^*, a_1^*, \boldsymbol{\lambda}^*, t) \leq \mathcal{H}(\mathbf{x}^*, a_1, \boldsymbol{\lambda}^*, t), \quad \forall t \in [t_0, t_f]. \quad (10)$$

Specifically, (10) can be decomposed into the following necessary conditions (for detailed derivations of these conditions, interested readers can refer to [28] and the references therein):

$$(i) \frac{\partial \mathcal{H}}{\partial a_1} = 0, \quad (ii) \dot{\boldsymbol{\lambda}} = -\frac{\partial \mathcal{H}}{\partial \mathbf{x}}, \quad (iii) \dot{\mathbf{x}} = \frac{\partial \mathcal{H}}{\partial \boldsymbol{\lambda}}, \quad (11)$$

where (11)(i) provides the optimal condition; (11)(ii) is the co-state equation; (11)(iii) characterizes the system dynamics.

(11)(i) can be rewritten as:

$$a_1(t) = -\lambda_2(t)/(2w_{21}). \quad (12)$$

The car-following behavior of the following HV, characterized by the GHR model, can be presented by:

$$a_2(t) = (v_1(t) - v_2(t))/\tau. \quad (13)$$

Substituting (13) into (11)(ii), we have:

$$\dot{\lambda}_1(t) = 0, \quad (14)$$

$$\dot{\lambda}_2(t) = -\lambda_1(t) - (\lambda_4(t) + 2w_{22}a_2(t))/\tau, \quad (15)$$

$$\dot{\lambda}_3(t) = 0, \quad (16)$$

$$\dot{\lambda}_4(t) = -\lambda_3(t) + (\lambda_4(t) + 2w_{22}a_2(t))/\tau, \quad (17)$$

Meanwhile, to enforce a desired final cost $\Phi(\mathbf{x}(t_f))$, the co-state $\boldsymbol{\lambda}$ at the final time t_f should meet the following condition:

$$\boldsymbol{\lambda}(t_f) = \frac{\partial \Phi(\mathbf{x}(t_f))}{\partial \mathbf{x}(t_f)}, \quad (18)$$

Recall that $a_1(t)$ is proportional to $\lambda_2(t)$ according to (12). Thus, solving for the optimal acceleration $a_1(t)$ is equivalent to solving $\lambda_2(t)$ from (14)–(18). However, we cannot get a general closed-form solution that simultaneously satisfies (15) at the start time t_0 (initial condition) and (18) (final condition).² The literature often resorts to numerical solutions using PMP, which solves the state $\mathbf{x}(t)$ forward in time according to (2) and (12), and propagates the co-state equations (14)–(17) backward in time. With iterations, total cost can converge to its minimum [30].

To address this problem, in the following analysis, we examine the analytical solutions under two specific conditions.

1) Analytical solution with $w_{22} = 0$:

To simplify the analysis, we firstly consider a special case where the energy consumption of the following vehicle is not included in the objective function, i.e., $w_{22} = 0$. We can derive the optimal acceleration of the lead CAV as follows.

Proposition 1. *If the lead CAV does not consider the energy consumption of the following vehicle, i.e., $w_{22} = 0$, the optimal acceleration of the lead CAV is:*

$$a_1(t) = \frac{w_{11} + w_{12}}{2w_{21}}(t_f - t) + \frac{\tau w_{12}}{2w_{21}}(e^{(t-t_f)/\tau} - 1). \quad (19)$$

The optimal acceleration has the following properties:

- (i) non-negative;
- (ii) decreases monotonically over time t ;
- (iii) increases with w_{11} or w_{12} , but decreases with w_{21} .

Proof. See Appendix C. □

As the optimal acceleration in (19) considers the travel distance of two vehicles but the energy consumption of the lead CAV only, the acceleration would be non-negative if there are no safety constraints for the lead CAV during the optimization horizon, i.e., Proposition 1(i). Meanwhile, a larger acceleration at the beginning of the optimization horizon can contribute more to the total travel distance of two vehicles. Therefore, the optimal acceleration keeps decreasing to reduce the energy consumption of the lead CAV, i.e., Proposition 1(ii). Moreover, Proposition 1(iii) is straightforward because a larger acceleration means a longer travel distance but more energy consumption.

²Malikopoulos & Zhao [29] derived a closed-form analytical solution for a single CAV, without considering following vehicles.

2) *Analytical solution with $a_1(t) = At + B + Ce^{Dt}$:*

In this subsection, we examine a more general case where the travel distance and energy consumption of both vehicles are taken into account, i.e., the full objective function (8) is minimized. Since the general solution cannot be obtained, we seek to derive the closed-form solution with a specified form. Inspired by the solution in Proposition 1, we assume the following composite form for the optimal acceleration of the lead CAV, i.e., a combination of linear function and exponential function with unspecified coefficients (A, B, C, D):

$$a_1(t) = At + B + Ce^{Dt}. \quad (20)$$

According to (4) and (12)–(18), we can solve for the coefficients A, B, C, D without considering constraints and obtain the following optimal solution (the detailed derivation process is relayed to Appendix D):

$$\begin{aligned} a_1(t) &= \frac{w_{11} + w_{12}}{2(w_{21} + w_{22})}(t_f - t) \\ &+ \frac{w_{12}\tau}{2(w_{21} + w_{22})} \left(e^{\sqrt{\frac{w_{21} + w_{22}}{\tau^2 w_{21}}}(t - t_f)} - 1 \right), \end{aligned} \quad (21)$$

under the condition that the initial speeds satisfy:

$$(v_1(0) - v_2(0)) / \tau = \varphi > 0, \quad (22)$$

where $v_1(0)$ and $v_2(0)$ are the initial speeds of the lead CAV and the following HV, respectively; $\varphi = \frac{\tau w_{11} + (w_{11} + w_{12})t_f}{2(w_{21} + w_{22})} + \frac{w_{12}\tau}{2w_{22}} e^{-\sqrt{\frac{w_{21} + w_{22}}{\tau^2 w_{21}}} t_f} \left(\sqrt{\frac{w_{21}}{w_{21} + w_{22}}} - \frac{w_{21}}{w_{21} + w_{22}} \right)$ is a constant related to exogenous parameters.

In the optimal solution (21), the first term comes from reducing the total cost of two vehicles without considering car-following behaviors, which is non-negative. The second term of (21) is associated with the car-following behavior of the following vehicle characterized by the GHR model. Since $t \leq t_f$, the second term is non-positive, which indicates that when taking into account the following vehicle's cost, the lead CAV should apply a smaller acceleration. One can readily verify that φ is always positive since $0 \leq \frac{w_{21}}{w_{21} + w_{22}} \leq 1$. Thus, (22) prescribes that the initial speed of lead CAV is larger than HV, i.e., $v_1(0) > v_2(0)$. A smaller acceleration considering the following HV in (21) can make a balance between improving the total travel distance and reducing the total energy consumption.

Noting that the optimal control (21) does not consider constraints, we further integrate constraints into the optimal control using the following lemma.

Lemma 1. *If $v_1(0) \geq v_2(0)$ and $a_1(t) \geq 0$ for all $t \in [0, t_f]$, the following vehicle modeled by the GHR model will never collide with the preceding CAV.*

Proof. See Appendix E. \square

According to Lemma 1, safety constraints will not be violated if the lead CAV has a larger initial speed and a non-negative acceleration during the whole optimization horizon. Moreover, non-negative acceleration will ensure the minimum acceleration and speed. Therefore, the optimal acceleration

of the lead CAV will only be bounded by the maximum acceleration and speed.

As (22) ensures a larger initial speed of the lead CAV, we present the following condition that the optimal acceleration of the lead CAV is always non-negative.

Remark 1. *The optimal acceleration $a_1(t)$ in (21) is non-negative if weighting factors satisfy: $\sqrt{\frac{w_{21} + w_{22}}{w_{21}}} \leq \frac{w_{11} + w_{12}}{w_{12}}$.*

Proof. See Appendix F. \square

It is noteworthy that the optimal acceleration $a_1(t)$ will be negative only under some extremely unbalanced settings of weighting factors. For example, $w_{22} \gg w_{21}$, where the lead CAV may decelerate considering the energy consumption of the following vehicle. With reasonable weighting factors, the optimal control $a_1(t)$ in (21) is non-negative, and has the following properties.

Remark 2. *If the optimal acceleration $a_1(t)$ in (21) is non-negative, $a_1(t)$ will:*

- (i) *increase with a larger w_{11} , but decrease with a larger w_{22} ;*
- (ii) *increase firstly and then decrease with a larger w_{12} ;*
- (iii) *may either decrease, or decrease firstly and then increase with a larger w_{21} ;*
- (iv) *decrease with a larger τ ;*
- (v) *decrease when taking into account more following HVs.*

Proof. See Appendix G. \square

Remark 2(i) is straightforward as a larger acceleration is helpful to improve the travel distance but will result in more energy consumption. As for Remark 2(ii), this is because a larger acceleration of the lead CAV can contribute more to the travel distance of the following HV. In the final stage of the optimization horizon, the optimal acceleration would decrease to save more energy consumption of the two vehicles. Remark 2(iii) dictates that the acceleration would become either smaller or smoother with a larger weighting factor for the energy cost of the lead CAV, i.e., w_{21} . Recall that τ is the adaptation time in the GHR model, and a larger τ represents a more conservative, or less sensitive driver of the following vehicle. A more conservative driver tends to adopt a smaller acceleration when following an accelerating vehicle. In this case, the optimal acceleration of the lead CAV should decrease to reduce the energy cost, i.e., Remark 2(iv). Remark 2(v) is because the lead CAV has a larger initial speed than the following HV(s). As a result, if the lead CAV considers the cost of more following HVs, the optimal acceleration would decrease to reduce the total energy consumption.

Notably, the analysis of $a_1(t)$ in Section II-B2 is derived based on the GHR car-following model and it is governed by condition (22). To investigate the relationship between the optimal acceleration and optimization parameters in more general settings, we conduct extensive numerical experiments with varying parameters and other car-following models, e.g., Appendix IV. Numerical results show that the optimal acceleration always increases when weighting factors for travel distance increase or weighting factors for energy consumption decrease, i.e., Remark 2(i)–(iii) always holds.

C. Numerical solution approach

The previous section examined the analytical property of the proposed control framework in a two-vehicle scenario. This section proceeds to investigate the general optimization problem in (3a) with constraints in (4)–(7). We firstly discretize the proposed continuous-time optimization problem and then present the solution approach to solve the problem in different traffic scenarios.

The proposed optimization problem presented in Section II-A is a quadratic programming problem with both linear and nonlinear constraints. To reduce the computation burden, the optimization problem is discretized by a time step dt . Then, the proposed optimization problem is transformed into a Mixed Integer Programming (MIP) problem that can be solved efficiently using numerical solvers, such as Gurobi [31]. The discretized optimization problem can be written as:

$$\begin{aligned} \min_{a_i, i \in N_c(t_0)} J &= (-w_1) \sum_{i=1}^{n(t_0)} d_i(N_{OH}) \\ &+ \sum_{i=1}^{n(t_0)} \sum_{k=1}^{N_{OH}} [w_2 a_i^2(k) + w_3 s_i^2(k) + w_4 l_i^2(k)], \end{aligned} \quad (23)$$

s.t.

$$d_i(k+1) = d_i(k) + v_i(k)dt + \frac{1}{2}a_i(k)dt^2, \forall i \in N(t_0), \quad (24a)$$

$$v_i(k+1) = v_i(k) + a_i(k)dt, \forall i \in N(t_0), \quad (24b)$$

$$d_{sig} - d_i(k) \leq M \cdot (1 - p_i), d_i(k) - d_{sig} \leq M \cdot p_i, \quad (24c)$$

$$\forall i \in N(t_0) \text{ and all } k \{k : sig(k) = red\}, \quad (24c)$$

$$d_i(1) = d_i(t_0), v_i(1) = v_i(t_0), \forall i \in N(t_0), \quad (24d)$$

$$(4)–(5) \text{ and } (7) \quad (24e)$$

where N_{OH} denotes the final time step in the optimization horizon; dt is the discretization time step. Slack variables s_i and l_i in (4)–(5) are penalized in the objective function with positive weighting factors w_3 and w_4 , respectively. (24a)–(24b) are the discretized form of the system dynamic (2). Signal constraint (6) is transformed to (24c) with the Big-M method, where M is a sufficiently large value and $p_i \in \{0, 1\}$ is the indicator variable of the vehicle i . Specifically, p_i equals one means that the vehicle i can pass the intersection during the current green phase and zero otherwise. Besides, initial states are constrained by (24d).

With the formulations in (23)–(24), the proposed optimization problem can be solved efficiently by numerical solvers in the MPC fashion. The optimization problem solves the optimal control for the whole optimization horizon, e.g., 10s, while only the optimized trajectories for the first 1s are implemented on controllable CAVs in the control corridor. The whole process updates every second according to the changing traffic states. In this way, the proposed control method only optimizes the trajectories of controllable CAVs inside the control corridor, i.e., between d^{start} and d^{end} .

To ensure computation efficiency while maintaining accuracy, the discretized time step in this paper is selected as one second ($dt = 1s$). Therefore, the size of the optimization problem depends on the optimization horizon T_{OH} . A longer

optimization horizon may achieve better optimization results but will lead to a longer computation time. To make a balance, we design a varying optimization horizon for scenarios with a signalized intersection, which is detailed below. For scenarios without intersection, a fixed optimization horizon is adopted.

As vehicles are not allowed to pass an intersection during red phases, improving the road throughput requires guiding more vehicles to pass the intersection in green phases. To improve the traffic throughput, we develop a varying optimization horizon for signalized scenarios. Specifically, at each optimization update, we set the optimization horizon to cover the current (or the upcoming) green phase, if the current phase is green (or red), respectively. For example, as shown in Fig. 2(a), assuming the duration of the green phase is t_g seconds, the optimization horizon should be $t_1 + t_g$ seconds if the current red phase lasts for t_1 seconds before changing to green. Whereas the optimization horizon is set as t_2 seconds if the current green phase remains t_2 seconds as in Fig. 2(b).

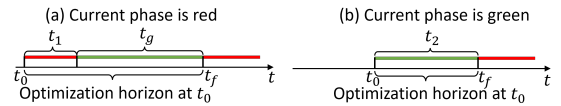


Fig. 2. Illustration of the varying optimization horizon.

The varying optimization horizon can maximize the number of vehicles passing the intersection with minimum energy cost in the current or upcoming green window. However, it only considers one signal cycle and thus there is always a red signal following the varying optimization horizon. A myopic CAV near the intersection may decelerate sharply when the signal turns from green to red. To avoid such unnecessary deceleration, we propose a green window allocation algorithm for each individual controllable CAV in the control corridor at each update. The pseudo-code of the green window allocation algorithm can be found in Appendix H.

Firstly, the proposed algorithm optimizes the trajectories of all vehicles in $N(t)$ for a varying optimization horizon t_f . Let $\{\mathbf{a}_i\}$ denote the acceleration of vehicle i . Then the control output \mathbf{U} includes acceleration of controllable vehicles predicted to pass the intersection. However, some controllable CAVs far away from the intersection cannot pass the intersection in the current optimization horizon. In this case, those CAVs will be allocated to the next green window. Specifically, for all vehicles that cannot pass the intersection, the algorithm will re-optimize their trajectories considering an extra signal cycle, i.e., $t'_f = t_f + t_r + t_g$, where t_r and t_g are durations of red and green phases, respectively. Then we can obtain the optimal control of all controllable CAVs by integrating the optimal control in the re-optimization into \mathbf{U} . Thanks to the green window allocation algorithm, all controllable CAVs inside the control corridor are assigned to a target green window, avoiding sharp deceleration approaching an intersection due to red signals.

III. NUMERICAL STUDIES

In this section, we evaluate the performance of the proposed method. Specifically, as shown in Fig. 1, we consider

a control corridor starting at 200m and ending at 1200m ($d_c^{start} = 200m$ and $d_c^{end} = 1200m$), where randomly distributed controllable CAVs and other vehicles drive east-bound. Two scenarios are investigated in this section. In the first scenario, we consider a traffic corridor with a signal at the end of the corridor. We test the proposed method with different proportions of controllable CAVs, possible vehicle permutations, and various levels of traffic intensity. Then, the proposed method is evaluated in a freeway scenario (without a traffic signal) with high traffic demand where congestion is likely to happen.

As mentioned in Section II, the GHR model leads to a small computation burden in solving the optimization problem due to its simplicity. However, it only considers the speeds of two consecutive vehicles and is unable to avoid rear-end collisions. In numerical studies, we simulate uncontrollable vehicles by a more complex but more accurate car-following model, i.e., the well-known IDM [32]:

$$a_i(t) = a \left[1 - \left(\frac{v_i(t)}{v_0} \right)^\delta - \left(\frac{s^*(v_i(t), \Delta v_i(t))}{s} \right)^2 \right], \quad (25)$$

where $s^*(v, \Delta v) = s_0 + \max \left\{ 0, vT_G + \frac{v\Delta v}{2\sqrt{ab}} \right\}$; a and b are the vehicle's maximum acceleration and comfortable deceleration, respectively; v_0 is the desired speed; δ is the acceleration exponent; s and $\Delta v_i(t)$ are the following distance and the speed difference between two adjacent vehicles, respectively; s^* is the desired distance; s_0 is the minimum spacing; T_G is the safe time gap. Notably, the IDM can also model uncontrollable vehicles' behaviors in response to traffic signals by setting a stationary vehicle at the stop line during the red signal. The parameters for simulation listed in Table I are adopted from [26], [32].

Thus, the more complex IDM is used to capture the driving behavior of uncontrollable vehicles in the simulation. Whereas the optimal control of controllable CAVs is solved using the GHR model taking advantage of its simplicity and solution efficiency. In Appendix I, we present the comparison of using GHR model to approximate the car-following behavior against the case where GHR model is used consistently in the simulation and optimization.

In the simulation, we use the Monte Carlo method to randomly generate controllable CAVs and other vehicles according to the given percentage of controllable CAVs. Moreover, mixed-autonomy traffic may exhibit varying complexities with various traffic demands. In particular, vehicles' arrival time at the initial point (0m) is modeled by the Poisson distribution related to the traffic demand [33]:

$$P(t = t_{enter}) = \frac{q^{t_{enter}} e^{-q}}{t_{enter}!}, \quad (26)$$

where $q = 1/Q_{demand}$; Q_{demand} is the traffic demand denoting the number of vehicles generated per hour; t_{enter} is the time step that a vehicle arrives at the zero point.

In the following numerical studies, a mixed traffic flow consisting of 50 vehicles is generated. Specifically, the first vehicle passes the zero point at 10m/s. Following preceding vehicles,

TABLE I
PARAMETERS FOR SIMULATIONS.

Variable	Description	Value
v_0	Desired speed	20m/s
s_0	Minimum spacing	2m
δ	Acceleration exponent	4
a	Maximum acceleration	1m/s ²
b	Comfortable deceleration	1.5m/s ²
T_G	Time gap in the IDM	1s
L	Vehicle length	5m
v_{max}	Maximum speed	20m/s
v_{min}	Minimum speed	0m/s
a_{max}	Maximum acceleration	1m/s ²
a_{min}	Minimum acceleration	-1.5m/s ²
τ	Adaptation time	4s
h	Time headway	1s (HVs follows HVs or CAVs) 0.5s (CAVs follow HVs) 0.1s (CAVs follow CAVs)

other vehicles pass the zero point at the time determined by (26) with the same speed as their immediate preceding vehicles. All simulations are conducted using MATLAB on a desktop computer with a Win-10 64-bit operating system and Intel(R) Core(TM) i7-9700 CPU 3.00GHz, 32G RAM.

A. A scenario with signalized intersections

In this scenario, as shown in Fig. 1, a signalized intersection locates at the end of the control corridor, i.e., 1200m. The signal follows a fixed time schedule. Specifically, in this paper, each signal cycle is 140s including 40s green phase and 100s red phase. The yellow phase is lumped with the red phase to ensure safety. Detailed SPaT settings are shown by red and green thick lines in Fig. 3. Extensive numerical studies are carried out under different traffic conditions, i.e., different proportions of controllable CAVs, possible permutations, and various traffic demands. The proposed method adopts the varying optimization horizon and green window allocation algorithm presented in Section II-C. The effects of incorporating these solution configurations are shown in Appendix I. Notably, for all the numerical results, the travel time, as well as the energy consumption, is calculated covering the whole control corridor, i.e., from 200m to 1200m.

1) Different proportions of controllable CAVs:

In this section, we test the proposed method under different percentages of controllable CAVs ranging from 0% to 100%, with an interval of 5%. For each controllable CAV percentage, we randomly generate 30 cases with 50 vehicles using the Monte Carlo method and evaluate the average performance of the proposed method. The traffic demand is set as 500 vehicles per hour.

Fig. 3 shows the trajectories of vehicles in 4 representative cases under 0%, 10%, 50% and 100% controllable CAVs. To clarify, the trajectories of controllable CAVs and other vehicles are shown by dashed lines and solid lines, respectively. As a baseline case, Fig. 3(a) shows trajectories of vehicles without controllable CAVs. It is observed that shockwaves form and propagate upstream during red signals. As a comparison, Fig. 3(b) shows trajectories of vehicles

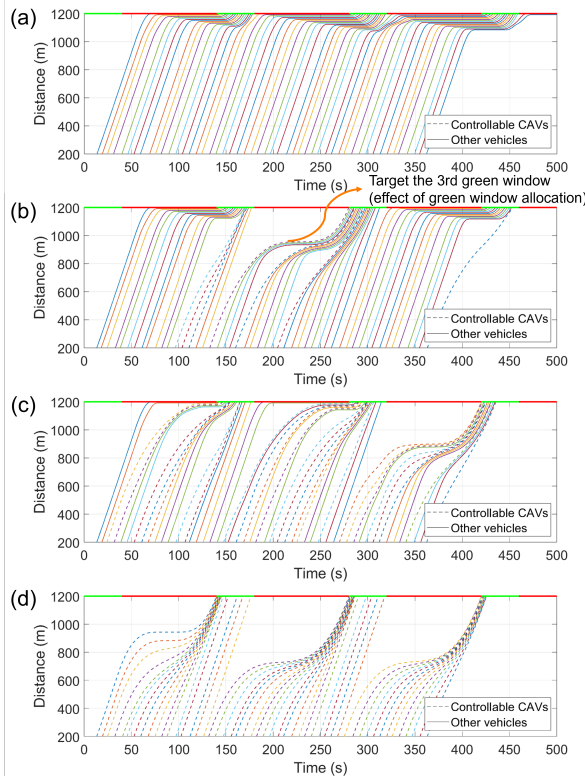


Fig. 3. Trajectories of vehicles in the scenario with a signalized intersection. (a) 0% controllable CAVs. (b) 10% controllable CAVs. (c) 50% controllable CAVs. (d) 100% controllable CAVs.

with 10% controllable CAVs. Clearly, CAVs can smooth the traffic flow when approaching the intersection because they can avoid unnecessary acceleration and deceleration with the SPaT information. Moreover, thanks to the allocation of green windows, CAVs will target the next green phase if they cannot pass the intersection during the current green phase (e.g., the CAV pointed by the orange arrow in Fig. 3(b)). Notably, two vehicles cannot pass the intersection before 500s without CAVs shown in Fig. 3(a). However, all vehicles can pass the intersection guided by controlled CAVs, even with a low proportion of controllable CAVs shown in Fig. 3(b). The fully controllable CAV environment shown in Fig. 3(d) has the largest road throughput because CAVs can drive within a safe but short car-following distance.

Fig. 4 shows the box and whisker plot for the 30 simulated cases under different proportions of controllable CAVs. Since controllable CAVs and other vehicles are generated by the Monte Carlo method according to the given proportion of controllable CAVs, the actual number of CAVs may fluctuate slightly at the same proportion. Meanwhile, even the number of controllable CAVs is the same, the permutations of CAVs may also affect the result, which is investigated in the following section. The legends in the box and whisker plots can be explained as follows (the same explanation applies to all box and whisker plots in this paper): the whiskers indicate the maximum and the minimum values; the bottom and top edges of the blue box indicate the 25th and 75th percentiles, respectively; the red central mark indicates the median, whereas the

black star mark shows the average. Therefore, a larger box and a longer whisker imply larger variations, indicating that the number of controllable CAVs and the CAV permutations would significantly affect the performance of the proposed method.

Fig. 4(a) presents the average travel time in the control corridor, which represents the traffic throughput (the first term in the objective function). Fig. 4(b) shows the energy consumption. Notably, as shown in Fig. 4(c), the average speed of all vehicles leaving the control corridor may be different, which may also affect energy consumption. For a fair comparison, we calculate the normalized energy consumption $E_{normal}(\mathbf{x})$ (in MJ) as the sum of the tractive energy and the kinetic energy gap [34], [35]. Specifically, as shown in (27), $E_{tractive}(\mathbf{x})$ is the calibrated energy consumption model presented in [5], which considers both the engine speed and gear position. The kinetic energy gap $\Delta E_{kinetic}(\mathbf{x})$ shown in (28) is the kinetic energy required to reach the free speed $v_0 = 20m/s$, where $m = 2000kg$ is the weight of vehicles; $v(t_f)$ is leaving speed of the vehicle; η is engine efficiency in transferring energy, which is set as 30% for internal combustion engine vehicles.

$$E_{normal}(\mathbf{x}) = E_{tractive}(\mathbf{x}) + \Delta E_{kinetic}(\mathbf{x}), \quad (27)$$

$$\text{with } \Delta E_{kinetic}(\mathbf{x}) = \frac{1}{2}m(v_0^2 - v(t_f)^2)/\eta. \quad (28)$$

The dashed line and dotted line in Fig. 4(b) show the average tractive energy and average kinetic energy gap under each percentage of controllable CAVs, respectively. Although the tractive energy may increase at a higher percentage of controllable CAVs, the normalized energy consumption always decreases with the increase of the controllable CAV percentage. Meanwhile, the travel time shown in Fig. 4(a) also decreases. Specifically, the travel time of all vehicles can be reduced by about 13% with 20% controllable CAVs and can be further reduced by 25% in a fully CAV environment. According to Fig. 4(a-c), we can infer that the proposed method can improve the throughput and simultaneously reduce the energy consumption of the mixed traffic flow.

Based on the traffic settings of this section, we also test the proposed method in a scenario with uncertainties. The relevant numerical results are presented in Appendix J.

2) Different permutations of CAVs in mixed traffic flow: As noted before, this section investigates how permutations of controllable and uncontrollable vehicles in the mixed traffic flow may affect the potential benefits. Fig. 5 shows the trajectories of vehicles in 4 representative cases selected from the total 30 simulated cases in Fig. 4 with 10% controllable CAVs. In all cases, the index of the controllable CAV is shown in the green box at the top of the figure. Accordingly, the performance of four cases is listed in Table II.

It is observed that, although CAVs can smooth the traffic flow in all cases, benefits in traffic and energy efficiency are different due to different CAV permutations. For example, there are 4 controllable CAVs in cases A-C, but Case A has the longest travel time, largest energy consumption, and smallest leaving speed. This is because a CAV (vehicle 10) in case A passes the intersection at the end of the green window.

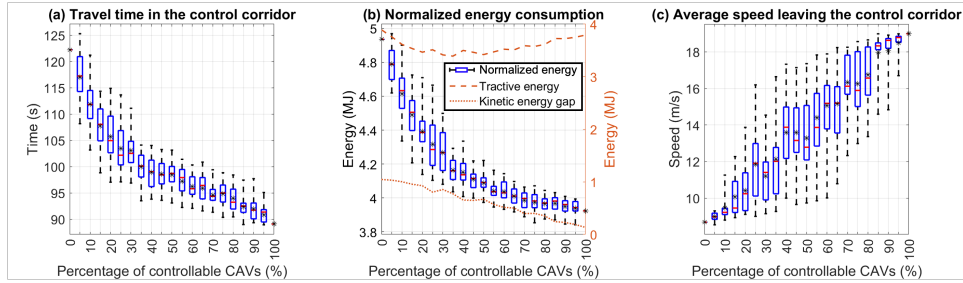


Fig. 4. Numerical results with different percentages of controllable CAVs in the scenario with a signalized intersection.

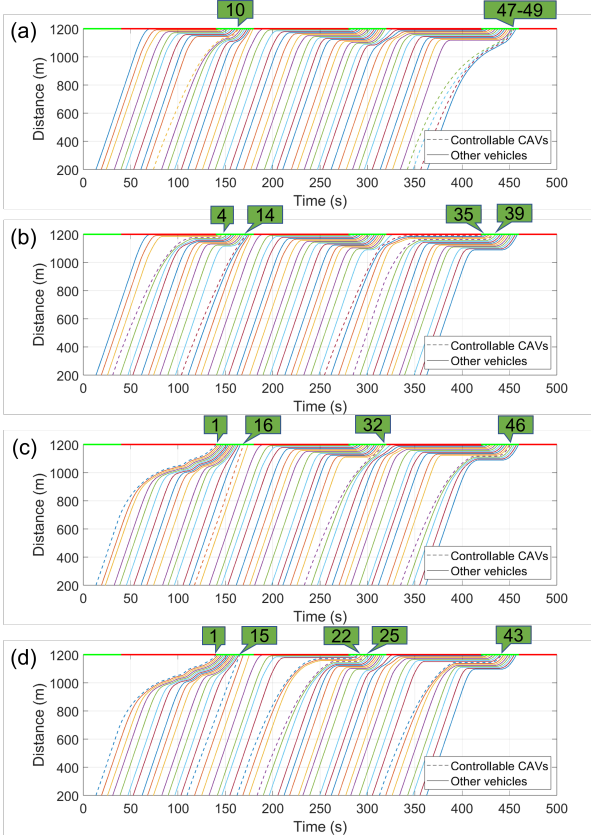


Fig. 5. Trajectories of vehicles with 10% controllable CAVs (Indexes of controllable CAVs are shown in the green boxes on the top). (a) Case A. (b) Case B. (c) Case C. (d) Case D.

Therefore, it can only guide a limited number of following vehicles to pass the intersections. Most following vehicles have to stop at the intersection due to red signals, forming a shockwave. When CAVs can lead more vehicles to pass the intersection (vehicle 4 in case B and vehicle 1 in case C), more benefits can be achieved, as shown in Fig. 5(b)–(c). Furthermore, case D has the best performance among all 4 cases because there are 5 CAVs (one more CAV compared with other cases) and CAVs pass the intersection at an earlier position in the mixed traffic flow during each green window compared with case C. The performance of individual vehicles is presented in Appendix K. It is observed that controllable CAVs may have small energy consumption and bring energy benefits to their following vehicles. Controllable CAVs may

TABLE II
PERFORMANCE OF CASES A-D

Case name	Travel time (s)	Normalized energy (MJ)	Average leaving speed (m/s)
Case A	114.58	4.706	9.09
Case B	113.82	4.677	9.25
Case C	112.60	4.658	10.23
Case D	109.15	4.582	10.35

TABLE III
DIFFERENT PERMUTATIONS OF CAVS IN MIXED TRAFFIC.

Index	Case name	Case descriptions
1	50HV	All 50 vehicles are uncontrollable
2	25HV-25ED	Controllable CAVs are evenly distributed in the last 25 vehicles
3	25ED-25HV	Controllable CAVs are evenly distributed in the first 25 vehicles
4	25HV-25CAV	The last 25 vehicles are controllable
5	25CAV-25HV	The first 25 vehicles are controllable
6	50ED	25 Controllable CAVs are evenly distributed in the 50 vehicles
7	50CAV	All 50 vehicles are Controllable CAVs

also have higher energy consumption when guiding many vehicles to pass the intersection, but the traffic and energy efficiency of the traffic flow can be improved.

Moreover, to further investigate the effect of vehicle permutations, we manually generate 7 cases with special controllable CAV permutations shown in Table III, where controllable CAV percentages are in ascending order.

Fig. 6 shows the performance of the proposed method in 7 cases. There are two findings regarding the CAV permutation. Firstly, more CAVs being downstream leads to a smaller travel time and a higher average leaving speed given the same proportion of controllable CAVs, e.g., case 3 versus case 2 and case 5 versus cases 4 and 6, as shown in Fig. 6(a) and (c). Secondly, evenly distributed CAVs in the mixed traffic flow are helpful to reduce energy consumption. If we compare cases 4-6 with 50% controllable CAVs in Fig. 6(b), case 6 has the largest energy benefits among them. Moreover, with evenly distributed CAVs, the energy consumption cost can be reduced by 17.6% when the percentage of controllable CAVs increases from 0% to 50%, i.e., case 1 to case 6. If the controllable CAVs percentage further increases from 50% to 100%, only another 3% reduction can be achieved, comparing case 6 with case 7. This implies that a half number of CAVs may achieve

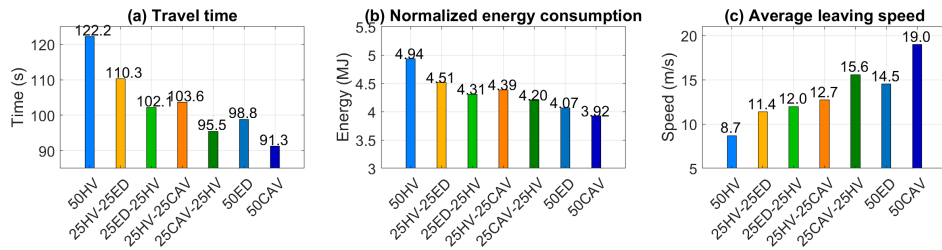


Fig. 6. Numerical results with different permutations of controllable CAVs in mixed traffic flow.

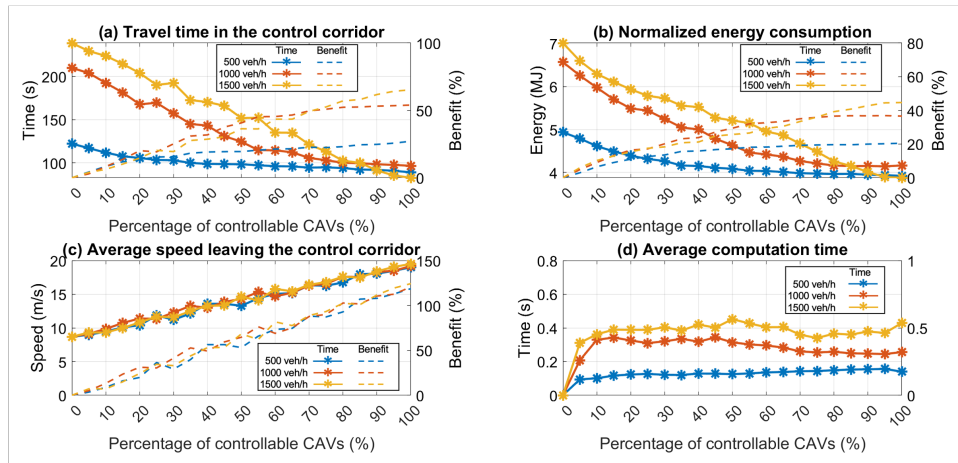


Fig. 7. Numerical results with different traffic demands in the scenario with a signalized intersection.

a similar performance in reducing energy consumption to a fully controllable CAV environment.

3) Different traffic demands:

Previous sections evaluated the proposed method at a constant traffic demand, i.e., 500 vehicles per hour. In the real world, the traffic demand varies in a day. For example, the traffic demand can be very high in rush hours, but low in off-peak periods. Given that the saturation flow is about 1400 vehicles per hour, this section investigates the performance of the proposed method with three different traffic demands, i.e., 500, 1000 and 1500 vehicles per hour, which can represent different traffic demand levels ranging from free to busy.

Fig. 7 shows the performance of the proposed method as well as the average computation time under three different traffic demands. In Fig. 7(a)–(c), the quantitative measurements are represented by solid lines (left y-axis) and the associated benefits compared with a 0% controllable CAV environment are shown by dashed lines in the same color (right y-axis). As shown in Fig. 7(a), with the proposed method, the travel time is similar in a fully CAV environment regardless of traffic demands. This is because CAVs can drive with a small car-following distance, allowing more CAVs to pass the intersection in the same green window. However, travel time is longer at a higher traffic demand when all vehicles are uncontrollable due to the limitation on throughput during green signals. Similarly, as shown in Fig. 7(b), energy consumption at 0% controllable CAVs is larger at higher traffic intensities, but they are similar under different traffic demands when the percentage of controllable CAVs is larger than 80%. It is also

observed that the proposed method can always achieve more than 40% total benefits in energy consumption with only 20% controllable CAVs. An additional 60% benefit can be achieved when the CAV percentage increases to 100%. These results show that significant benefits in traffic and energy efficiency can be achieved with the proposed method under various traffic demands.

Moreover, as shown in Fig. 7(c), the average speed leaving the control corridor keeps increasing with the controllable CAV proportion. However, the average leaving speeds of all vehicles appear to be similar under different traffic demands. This is due to that vehicles need to stop at the intersection because of red phases and do not accelerate until the signal turns green. Moreover, as shown in Fig. 7(d), the average computation time is always less than 0.5s. Since the proposed method is evaluated on a personal desktop written in MATLAB, the computation time can be further reduced by a high-performance computer. Therefore, the proposed method has the potential of being implemented in real-time.

B. A scenario without intersections

This section considers a traffic corridor on a freeway without signalized intersections. To better show the performance of the proposed method, the traffic demand is assumed to be 1500 vehicles per hour, which represents a high traffic demand. The proposed method is evaluated in different proportions of controllable CAVs. For each proportion, 30 random cases with 50 vehicles are generated using the Monte Carlo method. Notably, in all cases, the first vehicle is assumed to be an

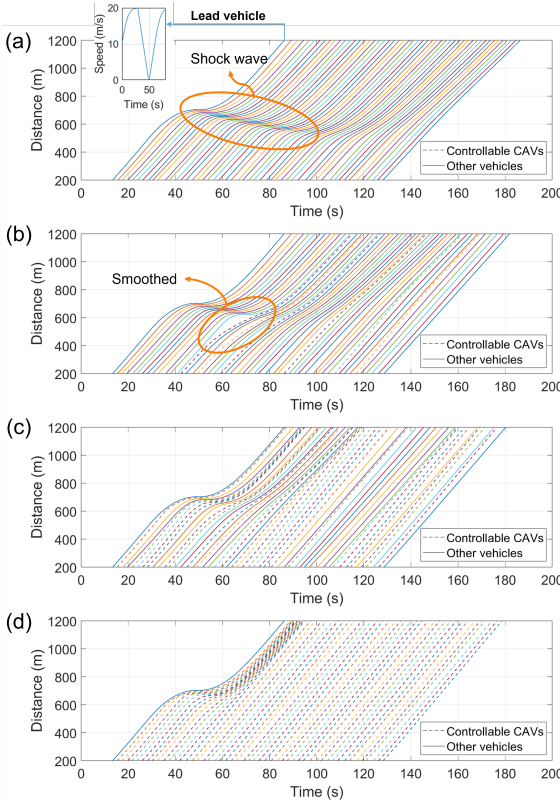


Fig. 8. Trajectories of vehicles in the scenario without intersections. (a) 0% controllable CAVs. (b) 10% controllable CAVs. (c) 50% controllable CAVs. (d) 100% controllable CAVs.

uncontrollable vehicle, which starts to decelerate for 20s at a constant deceleration -1m/s^2 as long as its speed reaches 20m/s . Moreover, as mentioned in Section II-C, the optimization horizon in (23) is set fixed at 20s to make a balance between the computation burden and seeking traffic and energy efficiency. Different lengths of the optimization horizon are compared in Appendix L.

Similar to Fig. 3, Fig. 8 shows the trajectories of all vehicles in 4 representative cases with different proportions of controllable CAVs (0%, 10%, 50%, and 100%), where controllable CAVs and other vehicles are presented by dashed lines and solid lines, respectively. Clearly, due to the deceleration of the first vehicle, the following vehicles have to decelerate to avoid rear-end collisions, forming a shockwave in Fig. 8(a). While CAVs upstream in Fig. 8(b) decelerate in advance when approaching the downstream shockwave at around 80s. A similar observation is found in Fig. 8(c) at around 60s, showing that the shockwave can be better smoothed at a larger proportion of controllable CAVs. When it comes to a fully CAV environment, the shockwave can be smoothed by the first few CAVs for two reasons. On the one hand, CAVs can decelerate in advance approaching the estimated shockwave. On the other hand, a controllable CAV adopts a smaller following distance when it follows a preceding CAV, which can absorb the shockwave.

Numerical results of the proposed method under various proportions of controllable CAVs are shown in Fig. 9. As shown in Fig. 9(a) and Fig. 9(c), with the increase of the

controllable CAV percentage, the average travel time keeps decreasing. At the same time, the average leaving speed of all vehicles keeps increasing, which implies a larger throughput of the road. Specifically, a fully CAV environment can reduce the travel time by about 22% and improve the average leaving speed by more than 8%, as against a 0% CAV environment. Meanwhile, Fig. 9(b) shows that the normalized energy consumption keeps decreasing with the increase of the percentage of controllable CAVs (both the tractive energy and the kinetic energy gap decrease). Compared with a 0% CAV environment, the energy consumption can be reduced by 23% when all vehicles are controllable CAVs. Moreover, the proposed method can achieve significant benefits in improving throughput and reducing energy consumption even at a low controllable CAV percentage. For example, when the percentage increases from 0% to 10%, the travel time and the energy consumption can be reduced by 6% and 10%, respectively. Hence, the traffic and energy efficiency is expected to be improved with limited controllable CAVs in the near future.

IV. CONCLUSION

This study investigates the potential of controlling a limited number of controllable CAVs in a mixed traffic corridor to improve traffic and energy efficiency. An efficient control method is developed to improve the overall traffic and energy efficiency by optimizing CAVs' trajectories without forming a platoon. We examine the analytical property of the proposed control method in an analytically tractable scenario with two vehicles. The proposed method is extensively evaluated in corridors with/without intersections under various conditions.

In a two-vehicle scenario where an HV follows a CAV, this paper derives the analytical optimal acceleration of the lead CAV under specific conditions. We find that the optimal acceleration is related to the intention of the proposed method. Generally, larger weighting factors for travel distance lead to a larger optimal acceleration. The optimal acceleration will decrease when more emphasis is put on reducing energy consumption. Moreover, the optimal acceleration may decrease if the following HV is more conservative or the lead CAV considers more following HVs.

In numerical studies, we evaluate the proposed control method in corridors with/without intersections, under different controllable CAV proportions and permutations, and various traffic demands. When the proportion of controllable CAVs increases from 0% to 100%, the total energy consumption can be reduced by around 45%, and at the same time the average travel time by more than 65%. Meanwhile, the average leaving speed of all vehicles is substantially enlarged, which indicates an improved traffic throughput. The proposed method can achieve significant benefits in traffic and energy efficiency with a limited proportion of controllable CAVs. For example, no more than 20% controllable CAVs can achieve half the benefits of a fully CAV environment. Notably, permutations of CAVs can affect the potential benefits of improving throughput and reducing energy consumption. It is observed that, with the proposed method, more benefits in traffic and energy efficiency can be achieved when controllable CAVs guide

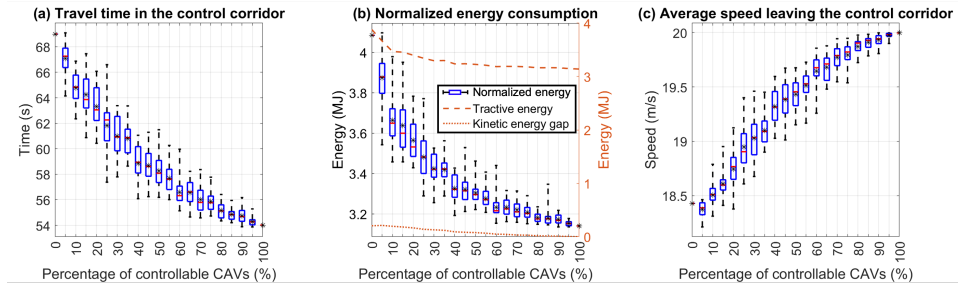


Fig. 9. Numerical results with different percentages of controllable CAVs in the scenario without intersections.

following vehicles to pass a signalized intersection in a green window. The traffic demand can significantly affect the travel time and energy cost of all vehicles in a fully uncontrollable environment. However, with the increase in the proportion of controllable CAVs, the traffic and energy performance tends to converge under different traffic demands. Regarding the computation efficiency, the average computation time of the proposed method is always below 0.5s, which can be further reduced by the high-performance computer, showing the great potential of the proposed method to be implemented in real-time.

This study can be fruitfully extended in different directions. Firstly, this study adopts the car-following models for uncontrollable vehicles. Specifically, we adopt the GHR model in the optimization problem to reduce the computation burden and the IDM in the simulation. However, all car-following models cannot fully capture uncontrollable vehicles' behaviors. For example, the GHR model does not consider the car-following distance, which also affects the acceleration of the following vehicle. Although numerical results show that the proposed method can achieve good performance in different traffic scenarios, more benefit is expected by improving the prediction model, e.g., adopting a more accurate car-following model with calibrated parameters for uncontrollable vehicles.

Secondly, this paper assumes that all vehicles drive in the same lane. Future studies may further integrate lane-changing models to predict lane-changing behaviors [36] and to optimize controllable CAVs' trajectories coping with lane changes [37]. The proposed framework may also be extended to consider a corridor with multiple lanes or a traffic network.

Thirdly, the signal follows a fixed schedule in this paper. As suggested by many studies [38], [39], traffic and energy efficiency can be improved by optimizing SPaT at intersections. To this end, it is expected that more benefits can be achieved by co-optimizing CAVs' trajectories and traffic signals. Moreover, the proposed method can consider optimizing CAVs' trajectories in all directions at a signalized intersection [8].

APPENDIX

The supplementary document can be found at www.xxxxxx.

REFERENCES

- [1] A. Talebpour and H. S. Mahmassani, "Influence of connected and autonomous vehicles on traffic flow stability and throughput," *Transportation Research Part C: Emerging Technologies*, vol. 71, pp. 143–163, 2016.
- [2] A. Vahidi and A. Sciarretta, "Energy saving potentials of connected and automated vehicles," *Transportation Research Part C: Emerging Technologies*, vol. 95, pp. 822–843, 2018.
- [3] W. Liu, "An equilibrium analysis of commuter parking in the era of autonomous vehicles," *Transportation Research Part C: Emerging Technologies*, vol. 92, pp. 191–207, 2018.
- [4] L. Li and X. Li, "Parsimonious trajectory design of connected automated traffic," *Transportation Research Part B: Methodological*, vol. 119, pp. 1–21, 2019.
- [5] Y. Shao and Z. Sun, "Vehicle speed and gear position co-optimization for energy-efficient connected and autonomous vehicles," *IEEE Transactions on Control Systems Technology*, vol. 29, no. 4, pp. 1721–1732, 2020.
- [6] *Taxonomy and Definitions for Terms Related to Cooperative Driving Automation for On-Road Motor Vehicles*, International SAE J3216_202107, 2021.
- [7] F. Ma, Y. Yang, J. Wang, X. Li, G. Wu, Y. Zhao, L. Wu, B. Aksun-Guvenc, and L. Guvenc, "Eco-driving-based cooperative adaptive cruise control of connected vehicles platoon at signalized intersections," *Transportation Research Part D: Transport and Environment*, vol. 92, 2021, Art. no. 102746.
- [8] W. Wu, Y. Liu, W. Liu, F. Zhang, V. Dixit, and S. T. Waller, "Autonomous intersection management for connected and automated vehicles: A lane-based method," *IEEE Transactions on Intelligent Transportation Systems*, vol. 23, no. 9, pp. 15091–15106, 2022.
- [9] W. Wu, F. Zhang, W. Liu, and G. Lodewijks, "Modelling the traffic in a mixed network with autonomous-driving expressways and non-autonomous local streets," *Transportation Research Part E: Logistics and Transportation Review*, vol. 134, 2020, Art. no. 101855.
- [10] Z. Chen, X. Lin, Y. Yin, and M. Li, "Path controlling of automated vehicles for system optimum on transportation networks with heterogeneous traffic stream," *Transportation Research Part C: Emerging Technologies*, vol. 110, pp. 312–329, 2020.
- [11] H. Jiang, J. Hu, S. An, M. Wang, and B. B. Park, "Eco approaching at an isolated signalized intersection under partially connected and automated vehicles environment," *Transportation Research Part C: Emerging Technologies*, vol. 79, pp. 290–307, 2017.
- [12] W. Zhao, D. Ngoduy, S. Shepherd, R. Liu, and M. Papageorgiou, "A platoon based cooperative eco-driving model for mixed automated and human-driven vehicles at a signalised intersection," *Transportation Research Part C: Emerging Technologies*, vol. 95, pp. 802–821, 2018.
- [13] X. Wen, Z. Cui, and S. Jian, "Characterizing car-following behaviors of human drivers when following automated vehicles using the real-world dataset," *Accident Analysis & Prevention*, vol. 172, 2022, Art. no. 106689.
- [14] Y. Guo, J. Ma, C. Xiong, X. Li, F. Zhou, and W. Hao, "Joint optimization of vehicle trajectories and intersection controllers with connected automated vehicles: Combined dynamic programming and shooting heuristic approach," *Transportation Research Part C: Emerging Technologies*, vol. 98, pp. 54–72, 2019.
- [15] M. Malekzadeh, I. Papamichail, M. Papageorgiou, and K. Bogenberger, "Optimal internal boundary control of lane-free automated vehicle traffic," *Transportation Research Part C: Emerging Technologies*, vol. 126, 2021, Art. no. 103060.
- [16] W. Sun, S. Wang, Y. Shao, Z. Sun, and M. W. Levin, "Energy and mobility impacts of connected autonomous vehicles with co-optimization of speed and powertrain on mixed vehicle platoons," *Transportation*

- Research Part C: Emerging Technologies*, vol. 142, 2022, Art. no. 103764.
- [17] S. Woo and A. Skabardonis, "Flow-aware platoon formation of connected automated vehicles in a mixed traffic with human-driven vehicles," *Transportation Research Part C: Emerging Technologies*, vol. 133, 2021, Art. no. 103442.
- [18] S. Gong and L. Du, "Cooperative platoon control for a mixed traffic flow including human drive vehicles and connected and autonomous vehicles," *Transportation Research Part B: Methodological*, vol. 116, pp. 25–61, 2018.
- [19] G. Piacentini, P. Goatin, and A. Ferrara, "Traffic control via platoons of intelligent vehicles for saving fuel consumption in freeway systems," *IEEE Control Systems Letters*, vol. 5, no. 2, pp. 593–598, 2020.
- [20] H. Shi, Y. Zhou, K. Wu, X. Wang, Y. Lin, and B. Ran, "Connected automated vehicle cooperative control with a deep reinforcement learning approach in a mixed traffic environment," *Transportation Research Part C: Emerging Technologies*, vol. 133, 2021, Art. no. 103421.
- [21] A. A. Malikopoulos, S. Hong, B. B. Park, J. Lee, and S. Ryu, "Optimal control for speed harmonization of automated vehicles," *IEEE Transactions on Intelligent Transportation Systems*, vol. 20, no. 7, pp. 2405–2417, 2018.
- [22] P. Typaldos, I. Papamichail, and M. Papageorgiou, "Minimization of fuel consumption for vehicle trajectories," *IEEE Transactions on Intelligent Transportation Systems*, vol. 21, no. 4, pp. 1716–1727, 2020.
- [23] Y. Guo, Q. Sun, Y. Su, Y. Guo, and C. Wang, "Can driving condition prompt systems improve passenger comfort of intelligent vehicles? a driving simulator study," *Transportation Research Part F: Traffic Psychology and Behaviour*, vol. 81, pp. 240–250, 2021.
- [24] M. Saifuzzaman and Z. Zheng, "Incorporating human-factors in car-following models: a review of recent developments and research needs," *Transportation Research Part C: Emerging Technologies*, vol. 48, pp. 379–403, 2014.
- [25] T. Forbes, H. Zagorski, E. Holshouser, and W. Deterline, "Measurement of driver reactions to tunnel conditions," *Highway Research Board Proceedings*, vol. 37, pp. 345–357, 1958.
- [26] Y. Wei, C. Avci, J. Liu, B. Belezamo, N. Aydin, P. T. Li, and X. Zhou, "Dynamic programming-based multi-vehicle longitudinal trajectory optimization with simplified car following models," *Transportation Research Part B: Methodological*, vol. 106, pp. 102–129, 2017.
- [27] L. S. Pontryagin, *Mathematical theory of optimal processes*. CRC press, 1987.
- [28] M. A. M. Zulkeffli, J. Zheng, Z. Sun, and H. X. Liu, "Hybrid powertrain optimization with trajectory prediction based on inter-vehicle-communication and vehicle-infrastructure-integration," *Transportation Research Part C: Emerging Technologies*, vol. 45, pp. 41–63, 2014.
- [29] A. A. Malikopoulos and L. Zhao, "A closed-form analytical solution for optimal coordination of connected and automated vehicles," *2019 American Control Conference (ACC)*, pp. 3599–3604, 2019.
- [30] S. Wang, M. W. Levin, and R. J. Caverly, "Optimal parking management of connected autonomous vehicles: A control-theoretic approach," *Transportation Research Part C: Emerging Technologies*, vol. 124, 2021, Art. no. 102924.
- [31] Gurobi Optimization, LLC, "Gurobi Optimizer Reference Manual," 2021. [Online]. Available: <https://www.gurobi.com>
- [32] M. Treiber and A. Kesting, "Traffic flow dynamics," *Traffic Flow Dynamics: Data, Models and Simulation*, Springer-Verlag Berlin Heidelberg, pp. 983–1000, 2013.
- [33] X. Chen, J. Yin, K. Tang, Y. Tian, and J. Sun, "Vehicle trajectory reconstruction at signalized intersections under connected and automated vehicle environment," *IEEE Transactions on Intelligent Transportation Systems*, pp. 1–15, 2022.
- [34] X. Qi, G. Wu, K. Boriboonsomsin, and M. J. Barth, "Data-driven decomposition analysis and estimation of link-level electric vehicle energy consumption under real-world traffic conditions," *Transportation Research Part D: Transport and Environment*, vol. 64, pp. 36–52, 2018.
- [35] R. Tu, L. Alfaseeh, S. Djavadian, B. Farooq, and M. Hatzopoulou, "Quantifying the impacts of dynamic control in connected and automated vehicles on greenhouse gas emissions and urban no₂ concentrations," *Transportation Research Part D: Transport and Environment*, vol. 73, pp. 142–151, 2019.
- [36] Y. Zhang, Q. Lin, J. Wang, S. Verwer, and J. M. Dolan, "Lane-change intention estimation for car-following control in autonomous driving," *IEEE Transactions on Intelligent Vehicles*, vol. 3, no. 3, pp. 276–286, 2018.
- [37] H. Kazemi, H. N. Mahjoub, A. Tahmasbi-Sarvestani, and Y. P. Fallah, "A learning-based stochastic mpc design for cooperative adaptive cruise control to handle interfering vehicles," *IEEE Transactions on Intelligent Vehicles*, vol. 3, no. 3, pp. 266–275, 2018.
- [38] H. Liu, X.-Y. Lu, and S. E. Shladover, "Traffic signal control by leveraging cooperative adaptive cruise control (cacc) vehicle platooning capabilities," *Transportation Research Part C: Emerging Technologies*, vol. 104, pp. 390–407, 2019.
- [39] M. W. Levin, J. Hu, and M. Odell, "Max-pressure signal control with cyclical phase structure," *Transportation Research Part C: Emerging Technologies*, vol. 120, 2020, Art. no. 102828.

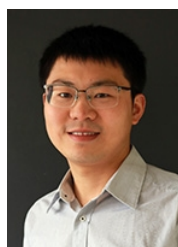
Wenbo Sun received the B.S. degree and M.S. degrees in automotive engineering from Beihang University in 2017 and 2020, respectively. He is currently pursuing the Ph.D. degree in transportation engineering at the University of Hong Kong. His main research interests include traffic control and operational research.



Fangni Zhang is an Assistant Professor at the Department of Industrial and Manufacturing Systems Engineering at The University of Hong Kong. Her research interests include shared transport and logistics systems, autonomous vehicle systems, transport network modeling and optimization, transport/urban data analytics.



Wei Liu is an Associate Professor and Presidential Young Scholar at the Department of Aeronautical and Aviation Engineering, The Hong Kong Polytechnic University. He mainly works on data-driven decision analytics, large-scale transport system modelling, optimisation and computing, aviation and rail system modeling, and transport economics.



Qingying He received her MSc degree in Computational Mathematics and Finance from the University of Edinburgh. She is a PhD candidate in transportation engineering at the Department of Aeronautical and Aviation Engineering, The Hong Kong Polytechnic University. Her PhD thesis was supervised by Dr. Wei Liu. Her research interests lie in transportation system modeling and optimization.



Optimal control of connected autonomous vehicles in a mixed traffic corridor

Wenbo Sun, Fangni Zhang

Department of Industrial and Manufacturing Systems Engineering, University of Hong Kong, Hong Kong

Wei Liu, and Qingying He

Department of Aeronautical and Aviation Engineering, The Hong Kong Polytechnic University, Hong Kong, China

APPENDIX A NOTATION LIST

TABLE A1
NOTATION LIST

Variable	Description
t	Time
T_{OH}	Length of the optimization horizon
T_{UD}	Update frequency of the optimal control
d_c^{start}	Start position of the control corridor
d_c^{end}	End position of the control corridor
$n(t)$	The number of vehicles in the control traffic stream
$N(t)$	Set of all vehicles in the control traffic stream at time t
$N_c(t)$	Set of CAVs in $N(t)$
$N_h(t)$	Set of HVs in $N(t)$
t_0, t_f	Start time and end time of the optimization horizon, respectively
d_{sig}	Location of the intersection (if exists)
$sig(t)$	Phase of the signal at time t (if exists)
t_r, t_g	Durations of red and green phases, respectively (if exists)
J	Objective function
Φ	Final cost function on travel distance in the objective function
\mathcal{L}	Energy consumption function in the objective function
w_1, w_2	Weighting factors for travel distance and energy consumption, respectively
w_3, w_4	Weighting factors to penalize violating car-following model and safety constraints, respectively
\mathcal{H}	Hamiltonian function
$\lambda(t)$	Co-state related to state $x(t)$
$u(t)$	Control input denoting acceleration of all CAVs in the control traffic stream at time t
$s_i(t)$	Slack variable for HV i at time t in the car-following model
$l_i(t)$	Slack variable for vehicle i at time t in the safety constraint
p_i	Binary variable, 1 if vehicle i can pass the intersection, and 0 otherwise
M	A sufficiently large value in signal constraints with the Big-M method
L	Vehicle length
$d_i(t)$	Location of vehicle i at time t
$v_i(t)$	Speed of vehicle i at time t
$a_i(t)$	Acceleration of vehicle i at time t
$x(t)$	State of all vehicles in the control traffic stream at time t
h	Time headway for a safe car-following distance
h_{min}	Minimum following distance when the vehicle is stationary
v_{max}	Maximum speed
v_{min}	Minimum speed
a_{max}	Maximum acceleration
a_{min}	Minimum acceleration
τ	Adaptation time of the following vehicle to reach the speed of its preceding vehicle
v_0	Desired speed of vehicles in the IDM model
s_0	Minimum spacing between two vehicles in the IDM model
δ	Acceleration exponent in the IDM model
a, b	Vehicle maximum acceleration and comfortable deceleration in the IDM model, respectively
T_G	Time gap in the IDM
η	Engine efficiency in transferring energy

APPENDIX B COMPARISON OF DIFFERENT WEIGHTING FACTORS FOR TRAVEL DISTANCE AND ENERGY CONSUMPTION

In Section III, we evaluate the proposed control framework with normalized weighting factors presented in Section II-A. Let \bar{w}_1 and \bar{w}_2 denote the normalized weighting factors, we compare the performance of the proposed methods with 5 different combinations of weighting factors shown in Table A2. Specifically, the third case is the same as the numerical results in Section III, i.e., the normalized weighting factors. Based on the third case, reducing energy consumption is more important in the first two cases while improving the travel distance is more essential in the last two cases. For fairness, the numerical results are conducted in a signalized scenario presented in Section III-A with traffic demand set at 500 vehicles per hour. Moreover, the permutation of controllable CAVs is fixed, where 10 controllable CAVs are evenly distributed in the traffic flow of 50 vehicles (20% controllable vehicles).

Fig. A1 and Table A2 show the results with different weighting factors for travel distance and energy consumption. The normalized energy consumption is presented in the table to make a fair comparison of all cases, and the tractive energy consumption is also presented in the table for reference. As shown in Table A2, when the optimal control emphasizes more on improving the travel distance (w_1 increases or w_2 decreases), the traffic throughput of the control corridor is improved (e.g., the travel time decreases and the average leaving speed increases comparing case W1 with case W3), and the normalized energy consumption increases (e.g., case W3 and case W5). It is also noted that compared with case W3, normalized energy consumption increases even if the proposed method emphasizes more on energy consumption in case W1. This is because controllable CAVs will avoid acceleration and deceleration if optimal control only considers reducing energy consumption. However, in the presence of the red signal, all vehicles have to stop. Although controllable CAVs can guide following vehicles to smoothly reduce speeds, they will also adopt smaller acceleration after the signal turns green. Therefore, for case W1 shown in Fig. A1(a), the average speed of all vehicles leaving the control corridor is low, which reduces the road throughput (longer travel time). Moreover, the lower average speed has a larger kinetic energy gap, resulting in more normalized energy consumption. Overall, the numerical results in Table A2 show that the normalized weighting factors used in Section III can make a balance

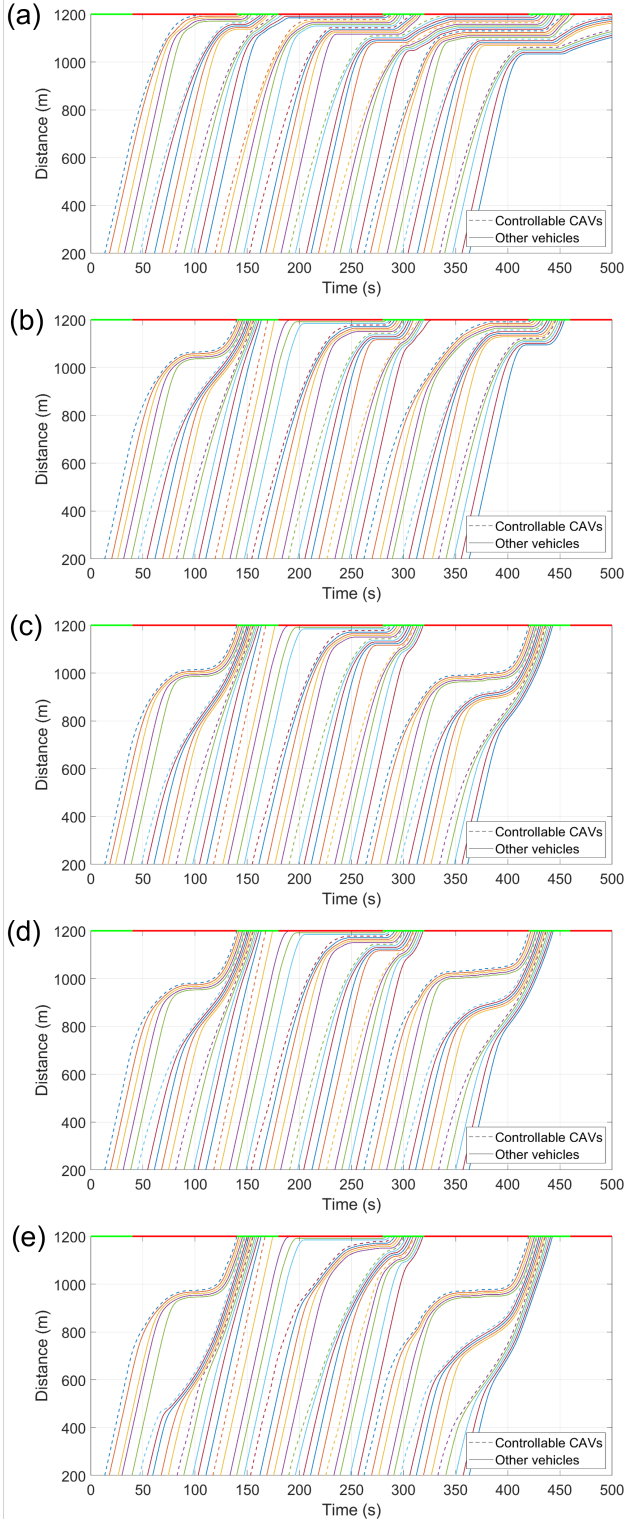


Fig. A1. Trajectories of vehicles with different weighting factors (20% controllable CAVs). (a) Case W1. (b) Case W2. (c) Case W3. (d) Case W4. (e) Case W5.

TABLE A2
PERFORMANCE OF DIFFERENT WEIGHTING FACTORS

Fig. A1 Case name	w_1	w_2	Travel time (s)	Normalized energy (MJ)	Traction energy (MJ)	Average leaving speed (m/s)
(a) W1	0	\bar{w}_2	163.19	5.19	3.96	4.80
(b) W2	$\frac{\bar{w}_1}{2}$	\bar{w}_2	108.23	4.34	3.43	10.65
(c) W3	\bar{w}_1	\bar{w}_2	103.46	4.35	3.68	13.62
(d) W4	\bar{w}_1	$\frac{\bar{w}_2}{2}$	103.78	4.40	3.73	13.67
(e) W5	\bar{w}_1	0	103.58	4.67	4.05	14.10

between road throughput and energy consumption.

C PROOF OF PROPOSITION 1

Proof. (19) can be obtained according to (12)–(18) with $w_{22} = 0$.

According to (19), $a_1(t) = -\frac{w_{11}+w_{12}-w_{12}e^{(t-t_f)/\tau}}{2w_{21}} < 0$ and $a_1(t_f) = 0$. Therefore, $a_1(t)$ is non-negative but keeps decreasing during the optimization horizon, and thus we have Proposition 1(i) and (ii).

Proposition 1(iii) can be obtained by noting $\frac{\partial a_1(t)}{\partial w_{11}} \geq 0$, $\frac{\partial a_1(t)}{\partial w_{12}} \geq 0$ and $\frac{\partial a_1(t)}{\partial w_{21}} \leq 0$. This completes the proof. \square

D ANALYTICAL SOLUTION WITH $a_1(t) = At + B + Ce^{Dt}$ IN THE TWO-VEHICLE SCENARIO

This appendix derives the optimal control shown in (21)–(22) assuming $a_1(t) = At + B + Ce^{Dt}$ with unspecified coefficients A, B, C, D .

A, B, C, D can be solved from (12)–(18). Specifically, with known $a_1(t)$, $\lambda_2(t)$ can be obtained according to (12). Then, $\lambda_4(t)$ can be solved from (15) (17), and (18). Further, we can obtain $a_2(t)$ from either (15) or (17). The unspecified coefficients A, B, C, D in $a_2(t)$ should satisfy the GHR model presented in (13), where speeds of two vehicles can be obtained by integrating the associated accelerations, i.e., $v_{\{1,2\}}(t) = v_{\{1,2\}}(t_0) + \int_{t_0}^t a_{\{1,2\}}(t')dt'$. Detailed process is shown below.

Given $a_1(t) = At + B + Ce^{Dt}$ and according to (12), $\lambda_2(t)$ can be written as:

$$\lambda_2(t) = -2w_{21}(At + B + Ce^{Dt}). \quad (\text{A1})$$

The derivative of (A1) with respect to time t is:

$$\dot{\lambda}_2(t) = -2w_{21}(A + CD)e^{Dt}. \quad (\text{A2})$$

Combining (15) and (17) gives $\dot{\lambda}_4(t) + \dot{\lambda}_2(t) = w_{11} + w_{12}$. Thus, $\lambda_4(t)$ can be solved by integrating $\dot{\lambda}_4(t)$ and letting it satisfy (18):

$$\lambda_4(t) = (w_{11} + w_{12})(t - t_f) + 2w_{21}(At + B + Ce^{Dt}). \quad (\text{A3})$$

With known $\dot{\lambda}_2(t)$ and $\lambda_4(t)$, $a_2(t)$ can be solved according to (15), which is:

$$a_2(t) = \frac{1}{2w_{22}} \left[\tau w_{11} - (w_{11} + w_{12})(t - t_f) - 2w_{21}(At + B + Ce^{Dt}) + 2\tau w_{21}(A + CD)e^{Dt} \right]. \quad (\text{A4})$$

Meanwhile, $v_1(t)$ and $v_2(t)$ can be obtained by integrating $a_1(t)$ and $a_2(t)$ while satisfying the initial states $v_1(0)$ and $v_2(0)$, respectively. Then, according to the GHR model shown in (4), $a_2(t)$ can also be written as:

$$a_2(t) = (v_1(t) - v_2(t)) / \tau \quad (\text{A5})$$

In this case, A, B, C, D can be solved by ensuring right hand sides of (A4) and (A5) equal, which is shown below:

$$\begin{aligned} \frac{1}{2w_{22}} & \left[\tau w_{11} + 2\tau w_{21}(A + CDe^{Dt}) - (w_{11} + w_{12})(t - t_f) \right. \\ & - 2w_{21}(At + B + Ce^{Dt}) \Big] = \frac{1}{2w_{22}} \left[(w_{11} + w_{12})(1/2t^2 - t_f t) \right. \\ & - w_{11}t - 2w_{21}(At + Ce^{Dt} - C) \Big] + \frac{1}{\tau} \left[v_1(0) - v_2(0) \right. \\ & \left. + (1/2At^2 + Bt + C(e^{Dt} - 1)/D)(1 + w_{21}/w_{22}) \right]. \end{aligned} \quad (\text{A6})$$

In case of $w_{22} \neq 0$, parts of undetermined coefficients (A, B, D) can be solved by letting first-order, second-order and exponential terms equal on the right and the left hand side of (A6). C is determined by (18). The solved A, B, C, D are:

$$A = -\frac{w_{11} + w_{12}}{2(w_{21} + w_{22})}, \quad (\text{A7})$$

$$B = \frac{(w_{11} + w_{12})t_f - w_{12}\tau}{2(w_{21} + w_{22})}, \quad (\text{A8})$$

$$C = e^{-\sqrt{\frac{w_{21}+w_{22}}{\tau^2 w_{21}}} t_f} \frac{w_{12}\tau}{2(w_{21} + w_{22})}, \quad (\text{A9})$$

$$D = \sqrt{\frac{w_{21} + w_{22}}{\tau^2 w_{21}}}. \quad (\text{A10})$$

Meanwhile, equalizing the constant terms in (A6) gives:

$$\begin{aligned} \frac{v_1(0) - v_2(0)}{\tau} &= \frac{\tau w_{11} + (w_{11} + w_{12})t_f}{2(w_{21} + w_{22})} + \\ & \frac{w_{12}\tau}{2w_{22}} e^{-\sqrt{\frac{w_{21}+w_{22}}{\tau^2 w_{21}}} t_f} \left[\sqrt{\frac{w_{21}}{w_{21} + w_{22}}} - \frac{w_{21}}{w_{21} + w_{22}} \right]. \end{aligned} \quad (\text{A11})$$

Let φ represent the right hand side of (A11). We can verify that $\varphi > 0$ because $0 \leq \frac{w_{21}}{w_{21} + w_{22}} \leq 1$, i.e., (22). To sum up, with (A11) being satisfied, the analytical solution (21) can be derived explicitly from (A7)–(A10).

E PROOF OF LEMMA 1

Proof. According to the GHR model, the following vehicle will have zero acceleration as long as it reaches the same speed as its preceding CAV. With a higher initial speed and non-negative acceleration, the lead CAV will always drive at a higher speed compared with the following vehicle, i.e., $v_1(t) \geq v_2(t)$ for all $t \in [t_0, t_f]$. Thus, two vehicles will not collide as the distance between two vehicles is non-decreasing during the optimization horizon $[0, t_f]$. This completes the proof. \square

F PROOF OF REMARK 1

Proof. Taking derivative of (21) with respect to time t gives:

$$\begin{aligned} \dot{a}_1(t) &= -\frac{w_{11} + w_{12}}{2(w_{21} + w_{22})} \\ & + \frac{w_{12}}{2\sqrt{(w_{21} + w_{22})w_{21}}} e^{\sqrt{\frac{w_{21}+w_{22}}{\tau^2 w_{21}}}(t-t_f)}, \end{aligned} \quad (\text{A12})$$

which increases over time t . When $t = t_f$, $\dot{a}_1(t_f) = \frac{-w_{11}-w_{12}+\sqrt{\frac{w_{21}+w_{22}}{w_{21}}}}{2(w_{21}+w_{22})}$. We can verify that $\dot{a}_1(t) \leq \dot{a}_1(t_f) \leq 0$ if $\sqrt{\frac{w_{21}+w_{22}}{w_{21}}} \leq \frac{w_{11}+w_{12}}{w_{12}}$, i.e., the acceleration is non-increasing during the optimization horizon. Moreover, as $a_1(t_f) = 0$, $a_1(t)$ is non-negative for all $t \in [0, t_f]$. This completes the proof. \square

G PROOF OF REMARK 2

Proof. Taking derivative of $a_1(t)$ with respect to w_{11} gives:

$$\frac{\partial a_1(t)}{\partial w_{11}} = \frac{t_f - t}{2(w_{21} + w_{22})} \geq 0. \quad (\text{A13})$$

Therefore, $a_1(t)$ increases with a larger w_{11} , i.e., the first part of Remark 2(i).

Taking derivative of $a_1(t)$ with respect to w_{12} gives:

$$\begin{aligned} \frac{\partial a_1}{\partial w_{12}} &= \frac{t_f - t}{2(w_{21} + w_{22})} \\ & + \frac{\tau}{2(w_{21} + w_{22})} \left[e^{\sqrt{\frac{w_{21}+w_{22}}{\tau^2 w_{21}}}(t-t_f)} - 1 \right]. \end{aligned} \quad (\text{A14})$$

Then, $\frac{\partial^2 a_1}{\partial w_{12} \partial t}$ can be calculated as:

$$\begin{aligned} \frac{\partial^2 a_1}{\partial w_{12} \partial t} &= \frac{-1}{2(w_{21} + w_{22})} \\ & + \frac{\sqrt{\frac{w_{21}+w_{22}}{w_{21}}}}{2(w_{21} + w_{22})} e^{\sqrt{\frac{w_{21}+w_{22}}{\tau^2 w_{21}}}(t-t_f)}, \end{aligned} \quad (\text{A15})$$

which increases with respect to time t . Noting that $\frac{\partial^2 a_1(0)}{\partial w_{12} \partial t} < 0$ and $\frac{\partial^2 a_1(t_f)}{\partial w_{12} \partial t} > 0$, $\frac{\partial a_1(0)}{\partial w_{12}}$ will decrease firstly and then increase with respect to time t . Moreover, as $\frac{\partial a_1(0)}{\partial w_{12}} > 0$ and $\frac{\partial a_1(t_f)}{\partial w_{12}} = 0$, $\frac{\partial a_1(t)}{\partial w_{12}}$ will be positive firstly and then negative in the optimization horizon $[0, t_f]$. In other words, with the increase of w_{12} , the acceleration of the lead CAV would increase firstly during the optimization horizon, but decrease at the later stage of the optimization horizon, i.e., Remark 2(ii).

Taking derivative of $a_1(t)$ with respect to w_{21} gives:

$$\begin{aligned} \frac{\partial a_1}{\partial w_{21}} &= \frac{(w_{11} + w_{12})(t - t_f)}{2(w_{21} + w_{22})^2} + \frac{w_{12}\tau}{2(w_{21} + w_{22})^2} \\ & \left[1 - e^{\sqrt{\frac{w_{21}+w_{22}}{\tau^2 w_{21}}}(t-t_f)} \left(1 + \frac{w_{22}}{w_{21}} \sqrt{\frac{w_{21} + w_{22}}{\tau^2 w_{21}}}(t - t_f) \right) \right]. \end{aligned} \quad (\text{A16})$$

Further, taking derivative of (A16) with respect to time t gives:

$$\frac{\partial^2 a_1}{\partial w_{21} \partial t} = \frac{(w_{11} + w_{12})}{2(w_{21} + w_{22})^2} - \frac{w_{12}\sqrt{\frac{w_{21}+w_{22}}{w_{21}}}}{2(w_{21} + w_{22})^2} \cdot e^{\sqrt{\frac{w_{21}+w_{22}}{\tau^2 w_{21}}}(t-t_f)} \left[1 + \frac{w_{22}}{w_{21}} \sqrt{\frac{w_{21}+w_{22}}{\tau^2 w_{21}}} (t-t_f) + \frac{w_{22}}{2w_{21}} \right]. \quad (\text{A17})$$

Note that the first term in (A17) is constant, whereas the second term will decrease firstly and then increase with respect to time t . Therefore, $\frac{\partial a_1(t)}{\partial w_{22}}$ gets the minimum value at either $t = 0$ or $t = t_f$. Since $\frac{\partial^2 a_1(0)}{\partial w_{21} \partial t} > 0$, we can discuss $\frac{\partial^2 a_1(t_f)}{\partial w_{21} \partial t}$ in two cases. On the one hand, if $\frac{\partial^2 a_1(t_f)}{\partial w_{21} \partial t} \geq 0$, $\frac{\partial^2 a_1}{\partial w_{21} \partial t} \geq \min \left\{ \frac{\partial^2 a_1(0)}{\partial w_{21} \partial t}, \frac{\partial^2 a_1(t_f)}{\partial w_{21} \partial t} \right\} \geq 0$, i.e., $\frac{\partial a_1}{\partial w_{21}}$ increases with respect to time t . Therefore, $\frac{\partial a_1(t)}{\partial w_{21}} \leq \frac{\partial a_1(t_f)}{\partial w_{21}} = 0$. In other words, the acceleration of the lead CAV would decrease with a larger w_{21} . On the other hand, if $\frac{\partial^2 a_1(t_f)}{\partial w_{21} \partial t} < 0$, $\frac{\partial a_1(t)}{\partial w_{21}}$ would increase firstly then decrease with respect to time t . Since $\frac{\partial a_1(0)}{\partial w_{21}} < 0$ (with a sufficiently large t_f) and $\frac{\partial a_1(t_f)}{\partial w_{21}} = 0$, $\frac{\partial a_1(t)}{\partial w_{21}}$ would be negative firstly and then positive in the optimization horizon, i.e., Remark 2(iii).

Taking derivative of $a_1(t)$ with respect to w_{22} gives:

$$\begin{aligned} \frac{\partial a_1}{\partial w_{22}} = & \frac{-1}{2(w_{21} + w_{22})^2} \left[(w_{11} + w_{12})(t_f - t) \right. \\ & + w_{12}\tau \left(e^{\sqrt{\frac{w_{21}+w_{22}}{\tau^2 w_{21}}}(t-t_f)} - 1 \right) \left. \right] \\ & + \frac{w_{12}e\sqrt{\frac{w_{21}+w_{22}}{\tau^2 w_{21}}}(t-t_f)}{4(w_{21} + w_{22})^2} \sqrt{\frac{w_{21}+w_{22}}{w_{21}}}(t-t_f). \end{aligned} \quad (\text{A18})$$

As the first term has the same sign as $(-a_1(t))$ which is non-positive and the second term in (A18) is also non-positive, we have $\frac{\partial a_1}{\partial w_{22}} \leq 0$ for all $t \in [0, t_f]$. Therefore, the optimal acceleration will decrease with a larger w_{22} , i.e., the second part of Remark 2(i).

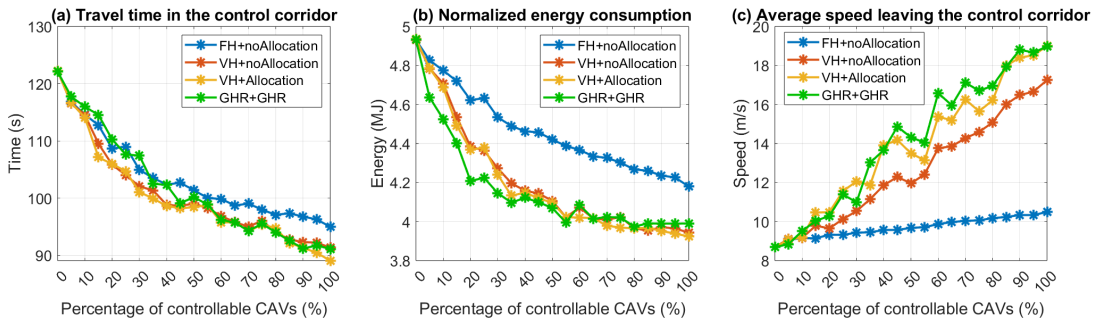


Fig. A2. Comparison of different solution configurations.

Moreover, taking derivative of $a_1(t)$ with respect to τ gives:

$$\begin{aligned} \frac{\partial a_1}{\partial \tau} = & \frac{w_{12}}{2(w_{21} + w_{22})} \cdot \\ & \left[e^{\sqrt{\frac{w_{21}+w_{22}}{\tau^2 w_{21}}}(t-t_f)} \left(1 - \sqrt{\frac{w_{21}+w_{22}}{\tau^2 w_{21}}}(t-t_f) \right) - 1 \right]. \end{aligned} \quad (\text{A19})$$

We can verify that $\frac{\partial a_1}{\partial \tau} \leq 0$ for all $t \in [0, t_f]$, i.e., Remark 2(iv).

It is noteworthy that more following HVs can be considered by improving w_{12} and w_{22} . For simplicity, we assume that all vehicles are assigned the same weighting factors for travel distance and energy consumption, i.e., w_1 and w_2 , respectively. The optimal control of the lead CAV considering n following HVs can be given by:

$$a_1(t) = \frac{w_1}{2w_2}(t_f - t) + \frac{nw_1\tau}{2(n+1)w_2} \left[e^{\frac{\sqrt{n+1}}{\tau}(t-t_f)} - 1 \right] \quad (\text{A20})$$

which decreases with respect to the number of following HVs n . Therefore, considering more HVs, the acceleration would decrease, i.e., Remark 2(v).

This completes the proof. \square

H GREEN WINDOW ALLOCATION ALGORITHM

See Algorithm A1.

I COMPARISON OF SOLUTION APPROACHES

In Section II-C, we propose the varying optimization horizon and the green window allocation algorithm for scenarios with signalized intersections. Then, Section III-A1 evaluates the proposed method in a signalized corridor under different proportions of controllable CAVs. With the same traffic settings as Section III-A1, Fig. A2 shows the numerical results with different solution configurations, i.e., fixed optimization horizon and without green window allocation (FH+noAllocation), varying optimization horizon and without green window allocation (VH+noAllocation), and varying optimization horizon and with green window allocation (VH+Allocation). Moreover, different from Section III, uncontrollable vehicles are simulated by the IDM, but are optimized based on the GHR model, a full-information simulation case is also shown in Fig. A2, where car-following behavior of uncontrollable vehicles is simulated by the GHR model (GHR+GHR).

Algorithm A1 Green window allocation.

```

1: Input:  $N(t)$ ,  $N_c(t)$ ,  $\mathbf{x}(t)$ 
2: Initialize  $U = \emptyset$ ,  $j = 0$ , and optimization horizon  $[t, t_f]$ 
3: Solve the optimization problem (23) for all vehicles in  $N(t)$  from  $t$  to  $t_f$ 
4: for  $i \in N_c(t)$  do
5:   if  $d_i(t_f) > d_{sig}$  then
6:     Update  $U = U \cup \{a_i\}$ 
7:   else
8:      $j = i$ 
9:     Break
10:    end if
11:   end for
12:   if  $j \neq 0$  then
13:      $N'(t) = \{j, j+1, \dots, n(t)-1, n(t)\}$  and  $N'_c(t)$  is the set of CAVs in  $N'(t)$ 
14:      $t'_f = t_f + t_r + t_g$ 
15:     Solve the optimization problem (23) for all vehicles in  $N'(t)$  from  $t$  to  $t'_f$ 
16:     for  $i \in N'_c(t)$  do
17:       Update  $U = U \cup \{a_i\}$ 
18:     end for
19:   end if
20: Output:  $U$ 

```

As shown in Fig. A2, although FH+noAllocation (the blue line) can achieve mobility and energy benefits, more benefits are achieved in VH+noAllocation (the red line) as it can make better use of SPaT information by adopting a varying optimization horizon. The green window allocation algorithm can further improve the benefits (the yellow line), especially in the average leaving speed shown in Fig. A2(c). This is because CAVs that cannot pass the intersection during the current green phase will decelerate in advance and target to pass the intersection during the next green phase at a higher speed. Moreover, the full-information case is shown in green. Since the GHR model only considers the speed difference but ignores the following distance of two consecutive vehicles, the GHR model may result in a smaller acceleration of the following vehicle compared with the IDM. For example, the vehicle modeled by the GHR model may not accelerate as long as it has the same speed as its preceding vehicle, even if the following distance is large. The smaller acceleration will lead to less energy consumption but longer travel time. Therefore, compared with yellow lines in Fig. A2(a-b), green lines have less energy consumption, but longer travel time, especially at a low proportion of controllable CAVs. The yellow and green lines always have similar trends, indicating that the proposed method can achieve benefits in traffic and energy efficiency even when the car-following model adopted in optimization is a simplification of the real-world car-following behavior.

J PERFORMANCE OF THE PROPOSED METHOD IN A SCENARIO WITH UNCERTAINTIES

In this appendix, we test the proposed method in a scenario with uncertainties. Specifically, the acceleration speed (m/s^2)

of uncontrollable vehicles is calculated by the IDM added a random value ϵ , i.e., given by (A21). Given that the minimum acceleration and maximum acceleration are $-1.5m/s^2$ and $1m/s^2$, respectively, the random value ϵ is set as following a uniform distribution in the interval of $[-0.05, 0.05]$.

$$a_i(t) = a \left[1 - \left(\frac{v_i(t)}{v_0} \right)^\delta - \left(\frac{s^*(v_i(t), \Delta v_i(t))}{s} \right)^2 \right] + \epsilon. \quad (\text{A21})$$

Fig. A3 compares the performance of the proposed method in scenarios with/without uncertainties. Based on the traffic scenario in Section III-A1, The red line and blue line represent the average performance with and without considering uncertainties in the IDM model, respectively. For a fair comparison, the permutations of controllable CAVs keep the same for all 30 simulated cases in each percentage of controllable vehicles. As shown in Fig. A3, when there are traffic oscillations, the throughput of the road may decrease (travel time increases and average leaving speed decreases), especially at a low percentage of controllable vehicles. The normalized energy consumption (solid line) is also higher under uncertainties, where both the tractive energy (dashed line) and the kinetic energy gap (dotted line) are higher under uncertainties shown in Fig. A3(b). Whereas the performances are similar at a high percentage of controllable vehicles because there will be less randomness. Importantly, it can be observed that the proposed method can handle traffic oscillations as it can improve road throughput and reduce energy consumption with a higher percentage of controllable vehicles.

K PERFORMANCE OF FIRST 18 VEHICLES IN FIG. 5

Table A3 lists the performance of individual vehicles in cases A–D shown in Fig. 5, in terms of the travel time (s), energy consumption (MJ), and average leaving speed (m/s) of each vehicle, respectively. The vehicle indexes are shown in the first column and underlined values are the performance of controllable CAVs. According to the numerical results, the first 17 vehicles can pass the intersection in the same green phase. To save space, only the first 18 vehicles are presented in the table. It can be observed that the controllable CAVs may have smaller energy consumption and can bring energy benefits to their following vehicles. For example, vehicle 4 in cases A–B. Moreover, the controllable CAVs may also have more energy consumption. This is because the CAV will adopt higher acceleration when guiding many vehicles passing the intersection, which is consistent with Remark 2(v). For example, vehicle 1 in cases C–D. The first few vehicles following the accelerating CAV may also have higher energy consumption. However, the whole traffic flow can achieve energy benefits and the road throughput can be improved. Comparing with vehicle 17, the travel time of vehicle 18 is substantially larger because it has to stop at the intersection.

L DIFFERENT OPTIMIZATION HORIZONS

In a corridor without signalized intersections, the proposed method adopts a fixed optimization horizon. The length of

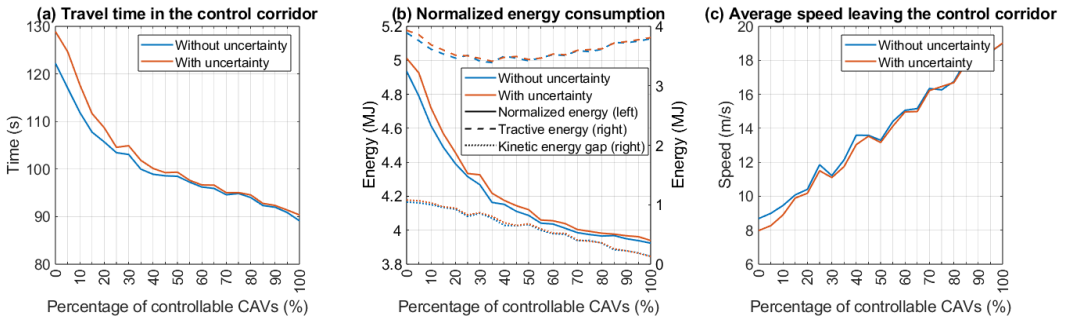


Fig. A3. Performance of the proposed method with uncertainties.

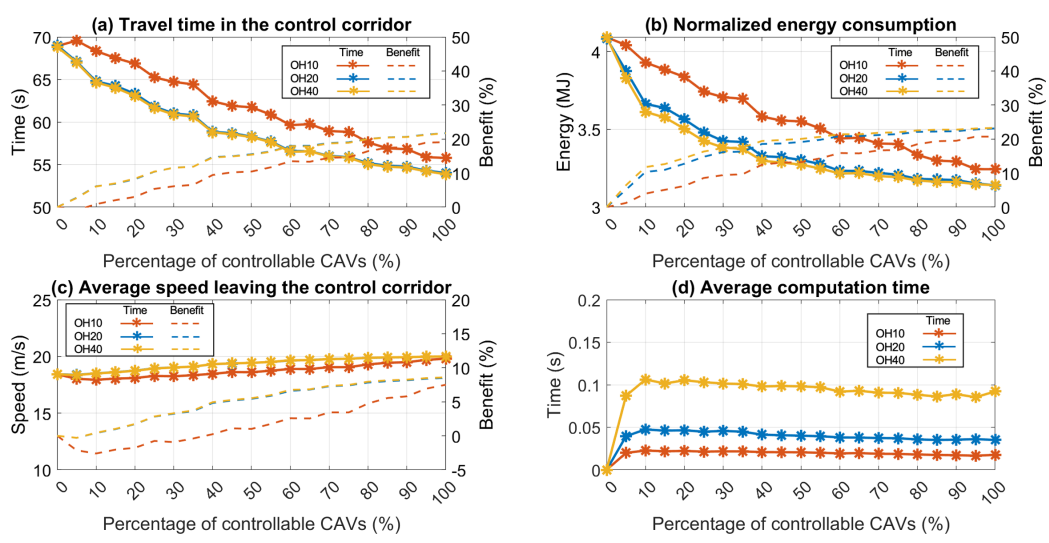


Fig. A4. Comparison of different lengths of the fixed optimization horizon.

TABLE A3
PERFORMANCE OF FIRST 18 VEHICLES IN CASES A-D OF FIG. 5

No.	Case A	Case B	Case C	Case D
1	126.5/5.0/1.9	126.5/5.0/1.9	126.7/5.1/9.7	126.7/5.1/9.4
2	124.7/4.9/4.1	124.6/4.9/4.1	122.8/4.9/10.0	122.8/4.9/9.6
3	122.7/4.9/5.4	121.4/4.8/5.4	120.6/4.9/10.4	118.3/4.9/9.9
4	117.2/4.7/6.5	<u>117.5/4.1/6.5</u>	113.0/4.8/10.6	114.9/4.9/10.3
5	113.0/4.7/7.3	112.5/4.4/7.4	109.1/4.9/11.1	109.2/4.9/10.6
6	110.5/4.7/8.1	107.0/4.5/8.1	103.9/4.8/11.3	102.6/4.8/10.9
7	104.7/4.6/8.7	104.3/4.5/8.8	97.9/4.8/11.7	98.9/4.8/11.2
8	99.6/4.6/9.4	97.7/4.5/9.5	92.0/4.7/11.9	91.3/4.7/11.4
9	96.5/4.5/10.0	92.7/4.5/10.0	87.8/4.6/12.2	87.3/4.6/11.7
10	<u>90.0/3.7/9.9</u>	89.6/4.5/10.6	82.3/4.4/12.4	82.9/4.4/11.9
11	83.6/3.9/10.9	85.2/4.4/11.1	74.5/4.2/12.7	75.9/4.3/12.2
12	79.2/4.0/11.4	79.2/4.3/11.6	70.5/4.2/12.9	71.0/4.2/12.4
13	74.3/4.1/11.9	73.3/4.2/12.0	65.7/4.0/13.2	65.8/4.0/12.7
14	69.3/4.1/12.2	<u>68.3/3.4/11.1</u>	58.2/3.4/13.5	61.0/3.8/12.8
15	64.4/4.0/12.5	62.9/3.4/12.0	53.7/3.0/15.7	<u>55.6/2.8/17.6</u>
16	58.3/3.7/12.7	57.2/3.3/12.6	<u>51.7/2.7/20.0</u>	51.4/2.8/19.4
17	53.4/3.1/15.8	53.3/3.1/15.5	50.7/2.7/19.9	50.3/2.7/19.9
18	148.1/5.2/1.9	148.3/5.2/1.9	146.9/5.2/1.9	147.1/5.3/1.9

Note: the numbers in the form of $a/b/c$ represent the travel time (s), energy consumption (MJ), and average leaving speed (m/s) of each vehicle, respectively. The underlined numbers represent controllable CAVs versus others representing uncontrollable vehicles.

the optimization horizon may also affect the performance of the proposed method. To examine this effect, Fig. A4 shows numerical results under different proportions of controllable CAVs with three different lengths of the optimization horizon, i.e., 10s (OH10), 20s (OH20), and 40s (OH40).

Generally, the longer the optimization horizon, the more future states can be optimized at the same time, leading to more benefits. On the contrary, controllable CAVs are myopic with a short optimization horizon. Therefore, as shown in Fig. A4(a) and Fig. A4(c), the travel time increases and the average leaving speed decreases in OH10 at low proportions of controllable CAVs. It is also observed that OH20 is much better than OH10 in reducing travel time and improving the average leaving speed. If the optimization horizon is further extended, the improvement becomes limited, e.g., OH40 has a similar performance to OH20 in Fig. A4(a) and Fig. A4(c). Moreover, as shown in Fig. A4(b), the longer the optimization horizon, the more benefits in reducing energy consumption. However, as expected, Fig. A4(d) shows that the average computation time increases with the length of the optimization horizon. In this paper, to balance the computation burden and potential benefits, the optimization horizon is set to be 20s for numerical studies in a corridor without signalized intersections.